Sortase-assembled pili promote extracellular electron transfer and iron acquisition in *Enterococcus faecalis* biofilm

Ling Ning Lam[1,2,7], Jun Jie Wong[1,3], Artur Matysik[1], Jason J. Paxman[4], Kelvin Kian Long Chong[1,5], Pui Man Low[1], Zhi Sheng Chua[1], Begoña Heras[4], Enrico Marsili[1,6] and Kimberly A. Kline[1,2,*]

[1]Singapore Centre for Environmental Life Science Engineering, Nanyang Technological University, 60 Nanyang Drive, Singapore 637551

[2]School of Biological Sciences, Nanyang Technological University, 60 Nanyang Drive, Singapore 637551

[3]Interdisciplinary Graduate School, Nanyang Technological University, Singapore 639798

[4]Department of Biochemistry and Genetics, La Trobe Institute for Molecular Science, La Trobe University, Science Drive, Bundoora VIC 3083, Melbourne, Australia

[5]Nanyang Technological University Institute for Health Technologies, Interdisciplinary Graduate School, Nanyang Technological University, 50 Nanyang Drive, Singapore 637553

[6]Department of Chemical and Materials Engineering, Nazarbayev University, 53 Kabanbay Batryr Avenue, Nur-Sultan 010000, Kazakhstan

[7]Department of Oral Biology, College of Dentistry, University of Florida, 1395 Center Drive, Gainesville, FL 32610, United States

*Correspondence: kkline@ntu.edu.sg

Keywords: *Enterococcus faecalis* biofilm, iron acquisition, endocarditis and biofilm associated pili, extracellular electron transfer, virulence

Classification: Biological Sciences, Microbiology

Abstract

Enterococcus faecalis is an opportunistic human pathogen and the cause of biofilm-associated infections of the heart, catheterized urinary tract, wounds, and the dysbiotic gut where it can expand to high numbers upon microbiome perturbations. The *E. faecalis* sortase-assembled endocarditis and biofilm associated pilus (Ebp) is involved in adhesion and biofilm formation *in vitro* and *in vivo*. Extracellular electron transfer (EET) also promotes *E. faecalis* biofilm formation in iron-rich environments, however neither the mechanism underlying EET nor its role in virulence was previously known. Here we show that iron associated with Ebp serve as a terminal electron acceptor for EET, leading to extracellular iron reduction and intracellular iron accumulation. We found that a MIDAS motif within the EbpA tip adhesin is required for interaction with iron, EET, and FeoB-mediated iron uptake. We demonstrate that MenB and Ndh3, essential components of the aerobic respiratory chain and a specialized flavin-mediated electron transport chain, respectively, are required for iron-mediated EET. In addition, using a mouse gastrointestinal (GI) colonization model, we show that EET is essential for colonization of the GI tract, and Ebp is essential for augmented *E. faecalis* GI colonization when dietary iron is in excess. Taken together, our findings show that pilus mediated capture of iron within biofilms enables EET-mediated iron acquisition in *E. faecalis*, and that these processes plays an important role in *E. faecalis* expansion in the GI tract.

Significance

Understanding enterococcal biofilm development is the first step towards improved therapeutics for the often antimicrobial resistant infections caused by these bacteria. Here we report a role for *Enterococcus faecalis* endocarditis and biofilm associated pili (Ebp) in mediating iron-dependent biofilm growth and contributing to extracellular electron transfer

(EET) which in turn promotes iron acquisition. Furthermore, we characterize the mechanisms underlying electron transfer in the *E. faecalis* biofilm. Our findings support a model in which *E. faecalis* use EET to drive the reduction of pilus-associated ferric iron, leading to iron acquisition in *E. faecalis* biofilm, and contributing to enterococcal virulence in the GI tract.

Introduction

Enterococcus faecalis is an important human opportunistic pathogen that causes a variety of diseases including endocarditis, urinary tract infections (UTI), bacteremia, wound infection, and medical device-associated infections [1]. Many of these infections are polymicrobial and biofilm-associated, rendering them more tolerant to antimicrobial and immune clearance, and contributing to their persistent nature [1]. Therefore, a detailed understanding of enterococcal biofilm development is a critical step towards advancing new therapeutics for treatment of these often antimicrobial resistant infections [1,2].

One important factor contributing to *E. faecalis* biofilm formation and virulence is the sortase-assembled endocarditis and biofilm associated pilus (Ebp) [3-7]. The importance of Ebp to *E. faecalis* is supported by the presence of its coding sequence in the core *E. faecalis* genome [5,8]. The Ebp fiber is primarily composed of the major pilin subunit EbpC, along with two dispensable minor pilin subunits EbpB and EbpA [5], and these pilin subunits are covalently assembled by Sortase C on the cell membrane, prior to attachment to the cell wall by Sortase A [6,9]. EbpA is the tip adhesin of the pilus, and its N terminus encompasses a metal ion-dependent adhesion site (MIDAS) motif. In eukaryotes, the MIDAS motif is important for ligand binding [10] and coordinates divalent cations, most often Mg^{2+} [11,12], for cell adhesion and interaction with extracellular matrix (ECM) proteins [12]. The MIDAS motif within the N-terminal domain of *E. faecalis* EbpA contributes to *in vitro* biofilm formation, adherence to

fibrinogen, and bladder colonization in a mouse catheter-associated urinary tract infection (CAUTI) model [13-15]. Sortase-assembled pili are conserved in many Gram-positive bacteria, where they often contribute to adhesion, biofilm formation, modulation of host immune response, and virulence [16,17]. The adhesive tips of these pilins (PilA of *Streptococcus agalactiae* [18], RrgA of *Streptococcus pneumoniae* [19], and AP-1 of *Streptococcus pyogenes* [20]) include a conserved von Willebrand factor A (vWFA) domain containing a MIDAS motif, which are essential for adhesion. However, the specificity and affinity for metal binding to the MIDAS motif in bacteria, including *E. faecalis,* has not been characterized.

Previously, we demonstrated that *E. faecalis* is electrogenic, and that iron promotes both extracellular electron transfer (EET) and biofilm growth in *E. faecalis* [21]. Several mechanisms for EET have been described in both Gram-positive and Gram-negative bacteria [22,23]. In some bacteria, microbial nanowires, composed of extracellular filamentous protein fibers and/or of cytochrome-associated fibers, have been proposed to aid EET by directly connecting the bacterial cell surface to extracellular metal oxides, or alternatively, by interacting with extracellular soluble redox mediators [23,24]. Biochemical and structural analysis have recently demonstrated that the conductive filaments of *Geobacter sulfurreducens* consist of polymerized chains of the hexaheme cytochrome OmcS [25]. Gram positive bacteria have evolved a highly conserved mechanism for EET, described in *L. monocytogenes*, which involves a specialized respiratory complex that channels electrons through discrete membrane-localized quinone pools to flavin intermediates, for subsequent delivery to terminal extracellular electron acceptors [26]. In *E. faecalis,* electroactivity requires the ability to synthesize L-lactate dehydrogenase (LDH) [21] and demethylmenaquinone (DMK) [27], important for catalyzing redox reactions and electron transfer during respiration, respectively [28].

In this study, we sought to understand the mechanism and physiological role of EET in *E. faecalis*. We show that EET in *E. faecalis* makes use of both DMK and the conserved flavin EET pathway described in *L. monocytogenes* for electron delivery to extracellular pilus-associated iron deposits. Iron induces the expression of Ebp pili, increasing the interaction sites for iron, which include the MIDAS motif of the EbpA tip adhesin, which is required for pilus association with iron as well as for iron-augmented biofilm formation. In addition, we show that EET drives the reduction of iron leading to FeoB-mediated uptake of iron into the *E. faecalis* biofilm cells. Finally, we demonstrate that a high iron diet promotes *E. faecalis* mouse gastrointestinal (GI) colonization in an *ebp*-dependent manner, and EET mutants are attenuated in the GI tract. Together, these findings suggest a model in which iron promotes pilus-mediated biofilm formation. We propose that the association of iron with sortase-assembled Ebp sequesters iron close to the cell surface within biofilms where it can serve as an extracellular electron acceptor for EET, resulting in the generation of ferrous iron for subsequent uptake into the cell. This new paradigm for iron acquisition in which pili and aggregates of piliated cells serve as iron sinks to promote biofilm formation and intracellular iron accumulation, significantly advances our mechanistic understanding of both biofilm formation and the pathogenesis of *E. faecalis*.

Results

Iron-augmented *E. faecalis* biofilm formation requires pilus expression

We previously demonstrated that *E. faecalis* biofilm growth in media supplemented with iron resulted in two-fold more biomass [21]. To test the hypothesis that Ebp contributes to iron-augmented biofilm, we performed biofilm assays in growth media supplemented with 2 mM ferric chloride ($FeCl_3$), and quantified total adherent biofilm biomass. In iron-supplemented

media, deletion mutants of the entire Ebp pilus (Δ*ebpABC)*, pilus tip (Δ*ebpA*) and pilus fiber (Δ*ebpC*) displayed more than a 50% reduction in biofilm growth compared to the wild type control **(Figure 1a)** and mutant biofilm levels in iron-supplemented media were most similar to wild type biofilm in the absence of iron augmentation **(Figure S1a)**. Biofilm formation by the pilus null Δ*ebpABC* mutant was restored to wild type levels upon genetic complementation with the full locus (p*ebpABCsrtC*). A Δ*ebpB* deletion mutant also displayed significantly reduced biofilm growth as compared to the wild type control in iron-supplemented media; however, it was not as strongly attenuated compared to the other pilus mutants **(Figure 1a)**. These findings are consistent with previous reports in which deletion of *ebpA* and *ebpABC* resulted in significantly reduced biofilm formation in normal media **(Figure S1a, S2b)** [6,29]. These results indicate that the fully assembled Ebp pilus fiber contributes substantially to iron-augmented biofilm formation with a key role for the EbpA pilus tip **(Figure 1a, S1b)**. We next tested the contribution of the MIDAS motif within EbpA to iron-mediated biofilm growth. Using a MIDAS mutant (*ebpA*^{AWAGA}), in which the native motif (Asp^{275}-Trp-Ser^{277}-Gly-Ser^{279}) is mutated to (Ala^{275}-Trp-Ala^{277}-Gly-Ala^{279}) [13], we observed that it was as attenuated as the *ebpABC* null mutant for biofilm formation in iron-supplemented media **(Figure 1a, S1a)**. Collectively, these data demonstrate that both the MIDAS motif of the EbpA tip adhesin, as well as an intact EbpC pilus fiber, are essential for iron-mediated biofilm growth.

Iron induces pilus expression and drives aggregation of pilus-expressing cells in *E. faecalis* biofilm

Iron-augmented *E. faecalis* biofilms have an altered 3-D structure [21]. To determine whether pilus expression contributes to the biofilm ultrastructure, we used immunofluorescence microscopy to visualize pilus-expressing cells within biofilms. Augmented biofilm biomass after growth in iron-supplemented media, as previously reported, was not apparent for the

Δ*ebpABC* or the *ebpA*^{AWAGA} mutants **(Figure 1b)** [21]. In addition, pilus-expressing cells tended to aggregate in areas of higher cell density in biofilms grown in iron-supplemented media **(Figure 1c)**. The abundance of piliated cell aggregates within the biofilm suggested that pilus expression may be induced in the presence of iron. We therefore quantified the number of biofilm cells expressing pili and observed a significantly larger pilus-expressing population in biofilms grown in ferric iron-supplemented media, but not in the presence of alternative iron sources or with other cationic metals **(Figure 1d)**. By contrast, we observed no significant difference in planktonically grown pilus-expression in response to iron **(Figure 1d)**. Together these results show that ferric iron induces pilus expression, which in turn increases the biofilm structure and mass.

Iron colocalizes with pili on the cell surface and is dependent on the EbpA MIDAS motif

While monitoring *E. faecalis* populations for piliation in iron-supplemented media, we observed dense deposits at the polar hemispheres of *E. faecalis* cells which co-localized with sites of EbpC deposition, suggesting that these dense deposits may be iron interacting with pili **(Figure 2a, Figure S2a-b)**. We observed these dense deposits less frequently in the *ebpA*^{AWAGA} mutant, even though this mutant strain expresses a similar proportion of piliated cells as WT **(Figure S2c),** and the dense deposits were completely absent in Δ*ebpABC* deletion mutant **(Figure 2a, Figure S2a-b)**, suggesting that pili may be interacting with ferric iron via the MIDAS motif of EbpA.

To confirm the interaction between the EbpA MIDAS motif and iron, we extracted Ebp from *E. faecalis* wild type and *ebpA*^{AWAGA} biofilms grown in normal or iron supplemented media, and in parallel performed control extractions from Δ*ebpABC* biofilms. Pili were isolated under native conditions and analyzed for iron content by inductive-coupled plasma mass

spectrometry (ICP-MS). Pilus extracts from wild type cells grown in the iron-supplemented media were associated with nearly three times more iron than wild type pilus extracts from biofilms grown in control media. Ebp association with iron was dependent on the EbpA MIDAS motif because pilus preps from *ebpA*^{AWAGA} were similar to background iron levels in control Δ*ebpABC* extracts **(Figure 2b)**.

To better understand how the EbpA MIDAS motif could interact with ferric iron, we modelled the EbpA structure based upon the crystal structures of its Mg bound homologs, *S. agalactiae* PilA GBS104 (PDB: 3txa) [30] and *S. pneumoniae* RrgA (PDB: 2ww8) [19]. The overall EbpA structural model (N177-P620) showed the expected vWFA structural fold encompassing the MIDAS motif, consistent with other pili tip adhesins **(Figure 2c-d)**. The model supports an interaction of the MIDAS motif and associated metal binding residues with ferric iron **(Figure 2e)**. D275 would make a water mediated contact with the iron, the hydroxyl oxygen atoms of S277 and S279 and the carboxylate oxygen of D378 would make direct ionic bonds with iron and the classic 6-coordination of iron would be completed by 2 water molecules. vWFA domains are known to undergo conformational changes from closed to open states, whereby iron bonding would be shifted from D378 to the nearby T350 [31]. The metal binding residues were confirmed by an alignment of the EbpA, GBS104 and RrgA sequences, which despite low sequence identity, showed strict conservation of the MIDAS motif D275, S277, S279, T350 and D378 residues **(Figure S3)**.

Pili and the respiration-associated electron transport chain contribute to extracellular electron transfer (EET)

The association of Ebp with iron, coupled with the ability of *E. faecalis* to undergo iron-mediated EET [21], suggested that pili themselves may be involved in the EET. To address this,

we measured the instantaneous current output by chronoamperometry and the cumulative charge production in biofilms grown in iron-supplemented media for 20 hours. We observed a reduction in cumulative charge production in both the Δ*ebpABC* and *ebpA*^{AWAGA} MIDAS mutants when grown in 0.5 mM iron-supplemented media **(Figure 3a)**. At higher iron concentrations, we did not observe significant differences in cumulative charge production over 20 hours **(Figure S4a)**. The current output in the first few hours was similar for all strains **(Figure S4b)**, but both pilin mutants exhibited an inability to sustain current output as compared to the wild- type control at later time points **(Figure S4a-b)**. We therefore conclude that pili contribute to sustained EET, but that other mechanisms also contribute to *E. faecalis* EET in the absence of the pili.

To identify additional pathways, in addition to pili, that contribute to iron-mediated EET, we examined the *E. faecalis* homolog of the *L. monocytogenes* EET-specific NADH dehydrogenase (*ndh3*) for flavin-mediated EET [26], as well as demethylmenaquinone (*menB*) for quinone-mediated EET [28]. We hypothesized that these electron transfer pathways may work together to promote EET. Indeed, we observed attenuated charge production in both *ndh3::Tn* and *menB::Tn* mutants [32,33] which was restored upon genetic complementation **(Figure 3b)**, as well as in mutants predicted to work in concert with Ndh3 in the conserved EET pathway **(Figure S5)**. Importantly, charge production was further reduced in the *ndh3::Tn* Δ*menB* double mutant compared to either single mutant **(Figure 3b),** suggesting that DMK and Ndh3 work in non-redundant concert for efficient EET**.** Together, these findings demonstrate that both respiratory electron transport conduits and pili contribute to iron-mediated EET in *E. faecalis* biofilm.

Genes encoding Ebp and the FeoB ferrous iron transporter are upregulated in *E. faecalis* biofilm

To further understand how iron promotes *E. faecalis* biofilm, we performed RNA sequencing and found a total of 90 genes that were differentially regulated upon growth in iron-supplemented media **(Table S1).** As expected, the pilus genes *ebpA* (OG1RF_RS04555) and *ebpB* (OG1RF_RS04560) were induced 1.68-fold and 1.55-fold respectively, which we validated by qRT-PCR **(Figure S6)**. Surprisingly, the only other iron-associated gene that showed both significant and differential expression was *feoB* (OG1RF_RS01950) encoding a predicted ferrous iron transporter, which was up-regulated 1.38-fold **(Table S1).** Importantly, this suggested that *E. faecalis* biofilm grown in iron-supplemented media may be importing ferrous iron. This finding was consistent with our earlier study that showed *E. faecalis* intracellular iron concentrations were increased in biofilm cells grown in iron-supplemented media [21]. The simultaneous up-regulation of *ebpABC* and *feoB* as the sole iron-responsive transporter, along with our observations that Ebp co-purify with iron and are required for EET suggested that pilus-associated iron may be reduced during EET and subsequently taken up by the ferrous iron transporter FeoB.

Extracellular ferric iron reduction replenishes ferrous iron pool for uptake by *E. faecalis* biofilm cells

Since ferric iron reduction to ferrous iron requires EET and is facilitated by both Ebp pili and the respiration electron transport chain, we predicted that an inability to perform EET would coincide with attenuation in ferric iron reduction and subsequent diminished extracellular ferrous iron pools available for uptake via FeoB. We therefore performed ICP-MS to determine the intracellular iron content in pilus mutants and EET-associated mutants grown in iron-supplemented media. Since Ldh1 was previously shown to be important for *E.*

faecalis EET [21], we predicted that the absence of *ldh1* may also lead to reduced intracellular iron accumulation. Consistent with these predictions, we observed significantly reduced intracellular iron for all pilus deletion mutants which was restored upon complementation, as well as reduced intracellular iron in the *ebpA*^{AWAGA} MIDAS and the *ldh1* mutants. Furthermore, we observed significantly reduced intracellular iron in the *ndh3::Tn* Δ*menB* mutant **(Figure 4a)**. As predicted, the absence of *feoB* also led to reduced intracellular iron, in a genetically complementable manner **(Figure 4b)**.

If intracellular ferrous iron accumulation is a direct consequence of EET catalyzed ferric iron reduction, EET mutants should display reduced ability for ferric iron reduction. We tested this using a ferrozine assay, which reacts with ferrous iron to form a stable colored product. With a functional EET mechanism, we predict the presence of increased ferrous iron pools. As expected, we observed a significant decrease in ferrous iron pools in *ldh1, ndh3* and *menB* mutants **(Figure 4c)**. Collectively, these data show that EET mutants are attenuated for ferric iron reduction and therefore intracellular iron accumulation.

Pili and respiration-associated electron transfer systems contribute to colonization of mouse GI tract

To understand how iron-augmented biofilms and EET impact *E. faecalis* pathogenesis, we examined the role of dietary iron in an antibiotic-treated mouse gastrointestinal (GI) colonization model. We fed mice a diet containing normal amounts of iron (control; 200 mg/kg ferric chloride) or excess iron (high iron; 2000 mg/kg ferric chloride), for 3 weeks prior to antibiotic exposure and subsequent ingestion of *E. faecalis* in the drinking water (**Figure 5a)**. Twenty-four hours after inoculation, we recovered significantly more *E. faecalis* from the mouse colon in mice fed the high iron diet as compared to the control group and this

increase was dependent on Ebp expression **(Figure 5b)**. Mice fed with high iron diet had increased levels of colon tissue-associated iron, which was not apparent in the cecum or small intestine **(Figure S7a)**. Accordingly, no iron-dependent colonization differences were observed in those compartments **(Figure S7b)**. These data suggest that dietary iron promotes *E. faecalis* Ebp-dependent colonization in the mouse colon. We next asked whether EET also provides a colonization advantage for *E. faecalis* in the GI tract. Indeed, both Ndh3 and MenB are required for GI colonization, independent of dietary manipulation **(Figure 5c, Figure S7c)**. Together, these findings demonstrate that both the pili and EET are important for GI colonization.

Discussion

We previously showed that *E. faecalis* performs EET in the presence of extracellular iron, which was associated with ATP production, and that iron supplementation augments biofilm growth [21]. In this study, we sought to understand the mechanism underlying EET and its physiological role in *E. faecalis*. We show that iron induces expression of the genes encoding the sortase-assembled Ebp, which in turn associate with iron via the MIDAS motif of the EbpA tip adhesin, and promote biofilm formation. We also show that EET is dependent on both DMK in the electron transport chain, and a specialized flavin-associated respiratory complex, leading to reduction of extracellular iron and FeoB-mediated uptake of iron (**Figure 6**). Furthermore, we demonstrate that pili are important for colonization in the iron-loaded mouse GI tract.

Many microorganisms have the capacity to generate electrical current via dissimilatory metal reduction [22,34,35]. In *E. faecalis*, it was previously known that EET relies upon DMK, part of its minimal electron transport chain [27], as well as Ldh1, involved in cellular redox

299 homeostasis [36]. Here we confirm that *menB*, required for DMK synthesis [37], contributes to
300 EET, along with a recently reported flavin-associated alternative membrane-bound electron
301 transport chain [26]. Since mutation of either pathway results in decreased charge production
302 and ferric iron reduction, whereas mutation of both pathways completely abrogates both
303 activities, we suggest that electrons flow through both respiratory complexes for maximally
304 efficient EET and ferric iron reduction. While the precise mechanism for electron transfer
305 outside of the *E. faecalis* cell may vary depending on the environmental niche, like *L.*
306 *monocytogenes* [26], *E. faecalis* is a flavin auxotroph [38], necessitating the presence of this
307 soluble electron shuttle in the vicinity of the microbes. Indeed, addition of riboflavin to *E.*
308 *faecalis* biofilms growing in microbial fuel cells augments current production [39]. Our work
309 also demonstrates that *E. faecalis* can use iron as a terminal acceptor for EET, which is likely
310 relevant both in the outside environment where Enterococci can persist for long periods of
311 time [40], as well as in the GI tract where less than 15% of dietary iron is absorbed at the
312 duodenum, leaving the majority destined for excretion [41] and potentially available for EET. In
313 addition, there are likely alternative terminal electron acceptors available for EET in the GI
314 tract, such as host associated iron, host-derived nitrate, or microbially-derived molecules such
315 as humic substances [42].
316
317 We previously demonstrated that *E. faecalis* biofilms, but not planktonic cells, grow better
318 upon iron supplementation [21]. We further showed that iron deposits accumulate in the *E.*
319 *faecalis* biofilm matrix [21], which is composed of extracellular DNA [43,44] as well as, most
320 likely, sortase substrates including Ebp that are continuously shed from wild type cells [6,9].
321 Here we show that the same pili are required for the formation of biofilm matrix-associated
322 iron deposits, and are both essential for iron-augmented biofilm formation and necessary for
323 EET. We speculate that Ebp contribute to EET in *E. faecalis* by sequestering iron as terminal

electron acceptors in close proximity to the cells, either as surface attached pili or within the tightly packed biofilm matrix, for efficient EET.

Both pilus associated EET and biofilm formation depend on an intact MIDAS motif within the EbpA pilus tip adhesin of a fully polymerized pilus. Ebp also co-purifies with iron in a MIDAS-dependent manner, demonstrating for the first time that the MIDAS motif contributes to the association of a protein with iron. Indeed, our structural model of EbpA aligns well with other pilus adhesin tips such as *S. agalactiae* GBS104 and *S. pneumoniae* RrgA, with a vWFA fold and MIDAS motif configured for binding cationic metals [76,77]. MIDAS motifs have been shown to bind a range of cationic metals, but in the case of EbpA this can include Fe^{3+} due to the local available concentrations in iron-rich environments. Apart from binding metals, MIDAS motifs also form part of substrate binding sites, whereby iron binding to this site could influence the interaction of EbpA with biofilm factors to promote an increase in biofilm mass [78]. Collectively, our data confirm that iron binding at the MIDAS motif has a dual role as both a terminal electron acceptor for EET and to promote biofilm formation. Moreover, vWFA domains can undergo conformational changes to open and closed states [78], so it is tempting to speculate that such a conformational change may have a role in the interaction with biofilm promoting factors and/or the release of iron after its reduction to Fe^{2+}.

Consistent with an important role for Ebp pili in an iron-rich environment, we show that the *ebp* operon is transcriptionally induced when iron is supplemented. Ebp are displayed on the surface of a subset of cells in any given *E. faecalis* population [5,6,9,29,45], and this population can be increased in the presence of serum [5] and bicarbonate [46]. Here we add another environmental signal, iron abundance, that can influence Ebp expression. Several intrinsic

349 factors can impact *ebp* gene expression including transcriptional regulators, EbpR [47], AhrC
350 (also annotated as ArgR3) and ArgR2 [48], the FsrB quorum sensing peptide [49] and the RNA
351 processing enzyme RNase J2 [50,51]. While none of these factors were differentially regulated
352 upon iron supplementation which may suggest uncharacterized regulatory pathways are
353 responsible for iron-regulated *ebp* transcription, we cannot rule out the possibility that excess
354 iron impacts the function of these known regulators of *ebp* expression.
355
356 In addition to *ebp*, the only iron-regulated *E. faecalis* gene annotated as iron-associated was
357 *feoB*, involved in ferrous iron uptake. Our discoveries that 1) Ebp expressing cells aggregate
358 within the biofilm, 2) *E. faecalis* accumulate intracellular iron in an Ebp-, EbpA MIDAS-,
359 and FeoB-dependent manner, and that 3) intracellular iron accumulation is abrogated in the
360 absence of EET and ability for ferric iron reduction, together suggest the presence of spatially
361 segregated areas within the biofilm that may be especially enriched for ferric iron
362 sequestration and reduction, subsequent ferrous iron acquisition, leading to biofilm growth
363 and restructuring. Our observation that *E. faecalis* can combine dissimilatory metal reduction
364 with iron acquisition is similar to early reports for *Shewanella putrefaciens* [52]. However, the
365 precise mechanism by which iron acquisition contributes to *E. faecalis* biofilm formation is
366 currently under investigation.
367
368 Enterococci are common but minor members of the GI microbiome. However, antibiotic
369 mediated dysbiosis favors overgrowth of Enterococci, harbouring both intrinsic and acquired
370 antibiotic resistance, in the lower GI tract [53-56]. In addition, their inherent tolerance to
371 oxidative stress [57] and high concentration of metals [21,58,59] can provide a selective advantage
372 for *E. faecalis* to colonize and bloom in niches unfavorable to other microbes. Our

observation that *E. faecalis* can both use EET and take advantage of iron-overload in the GI tract provides yet another mechanism by which *E. faecalis* can thrive in this niche.

Collectively, the findings of this study demonstrate that Ebp and EET facilitate iron reduction for its subsequent uptake, biofilm augmentation, and virulence in the antibiotic treated gut. Given the strong conservation of sortase-assembled pili containing MIDAS motifs in their tip adhesins among Gram positive pathogens, along with the conservation of genes encoding EET components in the same organisms, we propose that pilus-mediated metal capture and acquisition may be a common mechanism used by microbes to acquire limiting nutrients in a diversity of niches. This work therefore raises the possibility for new therapeutic strategies for *E. faecalis*, and potentially many other pathogens, aimed inhibiting extracellular electron flow, iron reduction and acquisition, and EET-associated ATP production.

Materials and Methods

Bacterial Strains and Growth Conditions. *E. faecalis* was grown in Brain Heart Infusion broth (BHI; Becton, Dickinson and Company, Franklin Lakes, NJ) and cultured at 37^{o}C under static or shaking (200rpm) conditions, as indicated. Preparation of inocula for biofilm and planktonic growth assays was performed as previously described following growth in Tryptic Soy Broth (TSB) or agar, supplemented with 0.175% glucose (TSBG) (Oxoid Inc., Ontario, Canada) [21]. Bacterial strains used in this study are listed in **Table S2.** Where appropriate, strains harbouring pGCP123 plasmids were grown in 1000 µg/mL kanamycin (Sigma Aldrich, USA) and strains harbouring pMSP3535 plasmids were grown in 100 µg/mL erythromycin unless stated otherwise. Metals were filtered sterilized and supplemented during medium preparation in autoclaved TSBG media. For experiments using ferric chloride only, metal is supplemented in TSBG media and autoclaved together. Ferric citrate hydrate

≥98%, magnesium chloride anhydrous ≥98%, copper chloride dihydrate ≥99%, ferrous sulphate heptahydrate ≥99%, ferric sulphate hydrate ≥97%, ferric chloride anhydrous ≥99%, heme ≥90%, and the chelator 2,2'dipyridyl ≥99% were all supplied by Sigma Aldrich, St Louis, MO, USA. Manganese chloride tetrahydrate and zinc chloride were supplied by Merk Millipore, Singapore.

General cloning techniques. Both *menB* and *ndh3* nucleotide sequences are based on the *E. faecalis* OG1RF genome obtained from BioCyc [60]. The Wizard genome DNA purification kit (Promega Corp., Madison, WI) was used for isolation of bacterial genomic DNA (gDNA), and Monarch® Plasmid miniprep Kit (New England BioLabs, Ipswitch, MA) was used for purification of plasmid for gene expression and construction of deletion mutant. The Monarch® DNA Gel Extraction Kit (New England BioLabs, Ipswitch, MA) was used to isolate PCR products during extension overlay PCR. In-Fusion HD Cloning Kit (TaKara Bio, USA) was used for fast, directional cloning of DNA fragments into vector for both expression vector and in-frame deletion vector. All plasmids used in the study are listed in **Table S3.** T4 DNA ligase and restriction endonucleases were purchased from New England BioLabs (Ipswitch, MA). Colony PCR was performed using Taq DNA polymerase (Thermo Fisher Scientific, Waltham, MA, USA) and PCR of gene of interest for plasmid construction was performed using Phusion DNA polymerase (Thermo Fisher Scientific, Waltham, MA, USA). Ligations were transformed into *E. coli* Dh5α cells. Plasmids derived in this study were confirmed by sequencing of purified plasmid.

Strain construction. To construct *menB* and *ndh3* complementation plasmids, primers (menB_F' and menB_R' for *menB*, or ndh3_F' and ndh3_R' for *ndh3*; **Table S3)** were designed with BamHI restriction site or SpeI restriction sites flanking the gene of interest, to

423 generate DNA fragments as templates for In-Fusion cloning (Takara Bio USA Inc.) using
424 primers (menB_F'_Infusion and menB_R'_Infusion for *menB*, or ndh3_F'_Infusion and
425 ndh3_R'_Infusion for *ndh3*) with at least 15 bp complementary sequence for ligation into the
426 nisin-inducible vector pMSP3535 digested with the same restriction enzymes. Both
427 pMSP3535::*menB* and pMSP3535::*ndh3* plasmids were generated in *E. coli* Dh5α, verified
428 by sequencing, and transformed into *E. faecalis* as described previously [13]. Deletion of the
429 *menB* coding sequence from the OG1RF chromosome was accomplished by allelic
430 replacement using pGCP213 temperature sensitive shuttle vector as described previously [13].
431 The deletion allele was constructed by extension overlap PCR, consisting of the upstream
432 (IFD_menB_Frag2_F' and IFD_menB_Frag2_R'; **Table S3)** and downstream
433 (IFD_menB_Frag1_F' and IFD_menB_Frag1_R'; **Table S3)** of the *menB* coding sequence,
434 and introduced into pGCP213 using in-fusion cloning with IFD_menB_Frag2_F' and
435 IFD_menB_Frag1_R' primers which has at least 15 bp complementary. Deletion of *menB*
436 was performed in *ndh3*::Tn parent strain to generate a double mutant. Transformants were
437 PCR screened for in-frame deletion as previously described [13].
438
439 **Immunofluorescence Imaging and 3D Reconstruction of Biofilm.** Bacterial cultures were
440 normalized to OD_{600} 0.7 and diluted 1000x prior inoculating into each well of μ-Slide 8 well
441 glass bottom slides (ibiTreat coated) (ibidi Inc., USA) containing 40% v/v TSBG for
442 incubation at 37°C under static conditions for 24 hours. After incubation, adherent biofilm
443 was fixed in 4% paraformaldehyde (Sigma Aldrich, USA)-PBS for 30 minutes, blocked with
444 3% bovine serum album (Sigma Aldrich, USA) (BSA)-PBS for 30 minutes, and incubated
445 with primary antibody (Rabbit Anti-Group D antigen, Thermo Scientific Singapore) or
446 Guinea Pig Anti-EbpC [45] at 1:500 dilution for 30 minutes. The biofilm was then washed with
447 3% BSA-PBS and incubated with secondary antibody (IgG horseradish peroxidase-

conjugated anti-rabbit or anti guinea-pig, Thermo Scientific Singapore) at 1:500 dilution for 30 minutes and washed with 3% BSA-PBS. Biofilms were hydrated with PBS prior to imaging. Biofilm morphology, biomass, and cell distribution were analysed by confocal laser scanning microscopy (CLSM). Images were acquired using LSM780 confocal microscope (Zeiss, Germany) equipped with 63x/1.4 Oil DIC M27 and controlled by ZEN software. Samples were illuminated with 488 nm and 561nm Argon laser line; GFP emitted fluorescence was collected in the 493-580 nm range and RFP emitted fluorescence was collected in the 568-712 nm range. Optical sections (134.95x134.95 µm) were collected every 0.637 µm through the entire biofilm thickness and signal from each section was averaged 4 times. Fiji software was used for further processing (levels adjustment, stack resliced). To visualize the biofilm spatial organization coordinates representing cocci position were plotted as spheres with cell-size diameter as described previously[21]. For each cell, local density was calculated as number of neighbour cells within 4µm radius, normalized and visualized using colour gradient.

Biofilm Assay. Bacterial cultures were normalized as previously described [21] and inoculated in TSBG in a 96-well flat bottom transparent microtiter plate (Thermo Scientific, Waltman, MA, USA), and incubated at 37^{o}C under static conditions for 5 days unless specified otherwise. Strains harboring pGCP123 complementation plasmids were grown in the presence of kanamycin prior to the biofilm assay, but kanamycin was not added to the biofilm assay itself because we found that kanamycin precipitates in the presence of excess iron leading to aberrant biofilm formation (data not shown). Adherent biofilm biomass was stained using 0.1% w/v crystal violet (Sigma-Aldrich, St Louis, MO, USA) at 4^{o}C for 30 minutes. The microtiter plate was washed twice with PBS followed by crystal violet solubilization with ethanol:acetone (4:1) for 45 minutes at room temperature. Quantification

473 of adherent biofilm biomass was measured by absorbance at OD_{595nm} using a Tecan Infinite
474 200 PRO spectrophotometer (Tecan Group Ltd., Männedorf, Switzerland).
475
476 **Planktonic Growth Assay.** Bacterial cultures were normalized as previously described [21]
477 and serially diluted by a dilution factor of 200. Diluted cultures were inoculated into the
478 media at a ratio of 1:25, which is 8 µL of the inoculum in 200 µL of media, incubated at 37°C
479 for 18 hours, and absorbance at OD_{600nm} was measured using a Tecan Infinite 200 PRO
480 spectrophotometer (Tecan Group Ltd., Männedorf, Switzerland) at 15 minute intervals.
481
482 **Population Analysis of Pilus Expression.** Biofilms were grown in 6 well tissue culture
483 plates at 37°C under static conditions for 24 hours in TSBG or TSBG supplemented with
484 metals where appropriate, and planktonic cultures were grown in 50-ml falcon tube under
485 shaking conditions (200 rpm). Immunoblotting was performed as described previously [61] with
486 some modification. Spent media was removed, and the adherent biofilm was suspended in
487 PBS. A cell scraper was used to dislodge the biofilm, and the dislodged cells were
488 centrifuged at 14,000 rpm for 2 minutes at room temperature to remove the supernatant.
489 Biofilm cells were suspended in PBS and normalized to OD_{600nm} 1.0. Normalized
490 suspensions were fixed in 4% paraformaldehyde (Sigma Aldrich, USA)-PBS for 20 minutes
491 at 4 °C, centrifuged at 14,000 rpm for 2 minutes. and the supernatant then discarded. The
492 pellets were washed with PBS, centrifuged at 14,000 rpm for 2 minutes, and the supernatant
493 discarded again. Immunofluorescence microscopy was performed as described previously [61]
494 with the following modifications: 1:500 dilution of guinea pig anti-EbpC (Thermo Scientific,
495 Singapore) in PBS-3% bovine serum albumin, and 1:500 dilution of goat Anti-guinea pig
496 AlexaFluor-568 (Invitrogen Inc., USA) incubation for 30 minutes. After washing with PBS
497 twice, resuspended cells were applied to poly-L-lysine slides (Polysciences Inc., USA), dried

for 5 minutes, mounted with Vectashield®, and sealed with a cover slip. Images were acquired using an inverted Epi-fluorescence microscope (Zeiss Axio observer Z1, Germany) equipped with an EC Plan-Neofluar 100x/1.3 Oil objective and controlled by ZEN software. For each biological sample, 5 images were acquired and the percentage of the cell population expressing pili was quantified. At least 300 bacterial cells per strain per experiment were scored for pilus expression. The metal concentrations used during the pilus expression experiments were based on the highest concentration in which *E. faecalis* cells did not exhibit growth inhibition (data not shown).

EbpA Structural Modelling. The EbpA amino acid sequence was submitted to the structural homology-modelling server Swiss-Model (https://swissmodel.expasy.org) [62]. Template structures for structural modelling were automatically selected based upon sequence identity. The initial template search derived 723 templates that were filtered down to 50 templates, whereby 14 models were constructed and ranked based on sequence similarity and coverage. The top solution was based upon the PDB 3txa (GBS104 from *Streptococcus agalactiae*) that showed 34% sequence similarity and 38% sequence coverage. The final EbpA model included N177-P620. The $Fe3^{+}$ was created with Sketcher [63] and placed into position using the MIDAS bound magnesium of 3txa and 2ww8 as a guide with the program COOT [64]. The two conserved water molecules from both 3txa and 2ww8 were fitted into EbpA by a similar means. Final alignments, analysis and structural figures were created with PyMOL [65].

Quantitative Real time PCR (qRT-PCR) and RNA sequencing. Biofilm cells were prepared as described above for TEM. After washing, the biofilm cell pellet was incubated with lysozyme from chicken egg white (10mg/ml) (Sigma Aldrich, USA) for 30 minutes at 37^{o}C to remove the cell wall and centrifuged at 14,000 rpm for 2 minutes at room

523 temperature to remove supernatant prior to cell lysis. RNA extraction was performed in a
524 Purifier® filtered PCR enclosure using the PureLink™ RNA mini kit (Invitrogen, USA)
525 according to the manufacturer's instructions. RNA purification and removal of DNA was
526 performed using TURBO DNA-free™ kit (Thermo Fisher, USA) and Agencourt®
527 RNAClean® XP Kit (Beckman Coulter, USA). Measurement of RNA yield and quality was
528 performed using Qubit® RNA HS assay kit (Thermo Fisher, USA) and RNA ScreenTape
529 System and 2200 TapeStation (Agilent, USA). Synthesis of cDNA was performed using
530 SuperScript III First-strand (Invitrogen, USA). Quantitative real-time PCR using cDNA was
531 performed using KAPA SYBR fast qPCR master mix kit (Sigma Aldrich, USA) and Applied
532 Biosystems StepOne Plus Real-Time PCR system. The expression of *ebpC*, *ebpR*, *srtA*, *srtC,*
533 *argR3* and *gyrA* were analysed using primer pairs listed in **Table S2**. For each primer set, a
534 standard curve was established using genomic DNA from *E. faecalis* OG1RF. Normalized
535 concentrations of cDNA were used to determine the relative fold change in gene expression
536 as compared to *E. faecalis* OG1RF biofilm grown in TSBG. For RNA sequencing, ribosomal
537 RNA depletion was performed after RNA purification using Ribo-Zero™ rRNA removal kit
538 (Illumina, USA). cDNA library synthesis was performed using NEBNext RNA First-strand
539 and NEBNext Ultra directional RNA Second-strand synthesis module (New England BioLab,
540 US). Transcriptome library preparation was performed using 300bp paired end Illumina
541 sequencing.
542
543 **Pilus Extraction and Purification.** Cell surface protein extracts from biofilms were prepared
544 as described previously [5] with minor modifications. Biofilms were grown cells dislodged as
545 described above for TEM. Dislodged biofilm cells were centrifuge at 3300 g for 4 minutes at
546 15^{o}C, washed with Tris buffer (10 mM Tris-HCl pH 8, 1 mM EDTA, 1 mM DTT) and
547 suspended in protoplast buffer with Pierce™ protease inhibitors (Thermo Scientific, USA).

548 Mutanolysin from *Streptomyces globisporus* ATCC 21553 (Sigma Aldrich, USA) and
549 benzonase nuclease (Sigma Aldrich, USA) were added and incubated at 37°C for 6 hours
550 with shaking (200 rpm). Following incubation, biofilm cells were centrifuged at 3300 g for 4
551 minutes, 15°C to obtain the supernatant. Supernatants were filtered through a 0.45µm Supor®
552 membrane (Sigma Aldrich, USA) and loaded into Corning Spin-X UF concentrators (MWCO
553 100kDa) (Sigma Aldrich, USA), centrifuged for 20 minutes, 15°C at 6000 g, and dialyzed
554 using Tris buffer using Spectra/Por® Float-A-Lyzer® G2 dialysis device (MWCO 300kDa)
555 (Spectrum Labs, USA). Pilus extracts were collected, quantified using Nanodrop 2000
556 Spectrophotometer (Thermofisher, USA), and normalized to 5 µg per sample. Samples were
557 mixed with an equal volume of NuPAGE® Tris-glycine native sample buffer (Novex®) and
558 loaded on to NuPAGE™ 3-8% Tris-acetate gel (Thermofisher, USA). Gel blots were run at
559 150 V for 3 hours. Western blotting was performed as described previously [6] with minor
560 modifications. Membranes were blocked in 0.05% v/v Tween-3% v/v bovine serum albumin-
561 PBS (Sigma Aldrich, USA) overnight at 4 °C and washed twice with 0.05% v/v Tween
562 (Sigma Aldrich, USA)-PBS prior to incubation with primary and secondary antibodies, and
563 prior to incubation with detection substrate. Primary antibody (guinea pig Anti-EbpC [45]or
564 rabbit Anti-SecA[6]) diluted 1:1500, and secondary antibody (IgG guinea pig or rabbit
565 conjugated horseradish peroxidase) diluted 1:4000 were used. Protein was detected using
566 SuperSignal® west femto maximum sensitivity substrate kit (Thermo Scientific, USA).
567
568 **Inductive-Coupled Plasma Mass Spectrometry (ICP-MS).** Pilus extracts, normalized to
569 5µg per sample, were run under native condition as described above. Using the western blot
570 prepared gel as a reference, a separate identical NuPAGE™ Tris-acetate gel (Thermofisher,
571 USA) was cut to isolate pilus extract ladder above a molecular weight of 100 kDa. At a ratio
572 of 2:1, 70% nitric acid (Sigma Aldrich, USA) and 30% hydrogen peroxide (Sigma Aldrich,

573 USA) was added to the excised gel slice containing the pilus protein, and left under room
574 temperature for 3 days to allow complete digestion. The digested samples were diluted with
575 LC-MS grade water and filtered using 0.2 µm membrane, prior to analysis using ICP-MS.
576 Analysis of trace metals in samples was performed using ICP-MS model Elan-DRCe,
577 Meinhard Nebulizer model TR-30-C3 (Perkin Elmer; Model: N8122006 (Elan Standard
578 Torch)).
579
580 **Electrochemical Assay and Analysis.** Screen printed electrodes (SPE) (model DRP-C110;
581 DropSens, Spain) consisting of a 4 mm diameter carbon working electrode, carbon counter
582 electrode, and a Ag pseudo-reference electrode were controlled by a multichannel
583 potentiostat (VSP, Bio-Logic, France) in an electrochemical cell of 9 mL working volume
584 sealed with a Teflon cap. Chronoamperometry was performed as previously described with
585 minor modifications [21]. All electrochemical experiments were conducted at 37^{o}C in TSBG
586 medium supplemented with 1 mM $FeCl_3$ unless otherwise stated.
587
588 **Ferrozine assay of ferric iron reductase activity.** *E. faecalis* cells were normalized to
589 OD_{600nm} 0.7, diluted 1:200 in PBS and resuspended in TSBG supplemented with 2 mM iron
590 (III) chloride as previously described [21] and then supplemented with 0.5 mM ferrozine.
591 Experiments were performed as previously described with minor modification [26]. $OD592_{nm}$
592 measurements were made every 2 mins for up to 7 hours on *E. faecalis* biofilms grown
593 statically. Corresponding change in optical density measurements correlates with color
594 change due to ferrous iron binding to ferrozine after ferric iron is reduced to ferrous iron.
595
596 **Mouse Gastrointestinal Tract (GI) Infection Model.** Three week old male C57BL/6NTac
597 mice were administered ampicillin (VWR, USA) in their drinking water (1 g/L) for 5 days as

598 previously described [53,55]. Mice were then given one day of recovery from antibiotic
599 treatment prior to administration of approximately 1-5 x 10^8 CFU/ml *E. faecalis* (OD_{600nm}
600 0.5) in the drinking water for 3 days as previously described [66]. Before and after infection,
601 mice were monitored for signs of disease and weight loss. All animal experiments were
602 approved and performed in compliance with the Nanyang Technological University
603 Institutional Animal Care and Use Committee (IACUC). For dietary manipulation,
604 customized synthesized diets (C1038 iron deficient diet with 200 mg/kg ferric chloride as
605 control diet, C1038 iron deficient diet with 2000 mg/kg ferric chloride as high iron diet)
606 (Altromin, Germany) were given to mice prior to infection and throughout infection. Mice
607 were kept on customized diets for 3 weeks before administrating ampicillin as previously
608 described with minor modification in the synthesized diet [67,68]. At the indicated timepoints,
609 the small intestine, colon, and cecum were harvested. Tissue samples were homogenised in
610 PBS, serial diluted in PBS, and spot-plated on BHI agar with 10 mg/L colistin, 10 mg/L
611 nalidixic acid, 100 mg/L rifampicin, 25 mg/L fusidic acid for CFU enumeration. All
612 antibiotics were obtained from Sigma Aldrich, USA.
613

614 **Authors Contributions**

615 L.N.L and K.A.K. conceptualized the study. L.N.L, E.M and K.A.K designed the
616 experiments, analyzed the data and prepared the manuscript. L.N.L performed biofilm
617 experiments, immuno-fluorescence assays, ICP-MS, and analyzed the data. A.M analyzed the
618 confocal data and generated 3D reconstruction models. LN.L, P.M.L., Z.S.C, and E.M
619 performed the electrochemistry experiments and analyzed the data. L.N.L and J.J.W
620 performed mouse GI experiments and analyzed the data. L.N.L prepared the RNA samples
621 for RNA sequencing and K.K.L.C analyzed the data. J.P. and B.H. performed modeling
622 experiments. All authors reviewed the manuscript.

Acknowledgments

This work was supported by the National Research Foundation and Ministry of Education Singapore under its Research Centre of Excellence Programme and by the Ministry of Education Singapore under its Tier 2 programme (MOE2014-T2-2-124). Artur Matysik was supported by the National Medical Research Council under its Clinical Basic Research Grant (NMRC/CBRG/0086/2015). We thank Wandy Betty (Washington University, St Louis, USA) for performing TEM, Hailyn V. Nielsen and Scott Hultgren (Washington University, St Louis, USA) for providing the pilus mutants, and Gary Dunny (University of Minnesota) for providing transposon mutants. Finally, we thank Sam Light and Dan Portnoy (University of California, Berkeley) for sharing unpublished data and for critical discussions of the manuscript.

References

1 Ch'ng, J. H., Chong, K. K. L., Lam, L. N., Wong, J. J. & Kline, K. A. Biofilm-associated infection by enterococci. *Nature reviews. Microbiology* **17**, 82-94, doi:10.1038/s41579-018-0107-z (2019).

2 O'Driscoll, T. & Crank, C. W. Vancomycin-resistant enterococcal infections: epidemiology, clinical manifestations, and optimal management. *Infection and drug resistance* **8**, 217-230, doi:10.2147/idr.s54125 (2015).

3 Nallapareddy, S. R. *et al.* Conservation of Ebp-type pilus genes among Enterococci and demonstration of their role in adherence of *Enterococcus faecalis* to human platelets. *Infection and immunity* **79**, 2911-2920, doi:10.1128/iai.00039-11 (2011).

4 Nallapareddy, S. R., Singh, K. V., Sillanpaa, J., Zhao, M. & Murray, B. E. Relative contributions of Ebp Pili and the collagen adhesin ace to host extracellular matrix protein adherence and experimental urinary tract infection by *Enterococcus faecalis* OG1RF. *Infection and immunity* **79**, 2901-2910, doi:10.1128/iai.00038-11 (2011).

5 Nallapareddy, S. R. *et al.* Endocarditis and biofilm-associated pili of *Enterococcus faecalis*. *The Journal of clinical investigation* **116**, 2799-2807, doi:10.1172/jci29021 (2006).

6 Nielsen, H. V. *et al.* Pilin and sortase residues critical for endocarditis- and biofilm-associated pilus biogenesis in *Enterococcus faecalis*. *Journal of bacteriology* **195**, 4484-4495, doi:10.1128/jb.00451-13 (2013).

7 Singh, K. V., Nallapareddy, S. R. & Murray, B. E. Importance of the ebp (endocarditis- and biofilm-associated pilus) locus in the pathogenesis of *Enterococcus faecalis* ascending urinary tract infection. *J Infect Dis* **195**, 1671-1677 (2007).

8 Sillanpää, J., Xu, Y., Nallapareddy, S. R., Murray, B. E. & Höök, M. A family of putative MSCRAMMs from *Enterococcus faecalis*. *Microbiology* **150**, 2069-2078, doi:doi:10.1099/mic.0.27074-0 (2004).

9 Kline, K. A. *et al.* Mechanism for sortase localization and the role of sortase localization in efficient pilus assembly in *Enterococcus faecalis*. *Journal of bacteriology* **191**, 3237-3247, doi:10.1128/JB.01837-08 (2009).

10 Plow, E. F., Haas, T. A., Zhang, L., Loftus, J. & Smith, J. W. Ligand Binding to Integrins. *Journal of Biological Chemistry* **275**, 21785-21788, doi:10.1074/jbc.R000003200 (2000).

11 Bergelson, J. M. & Hemler, M. E. Integrin-ligand binding. Do integrins use a 'MIDAS touch' to grasp an Asp? *Current biology : CB* **5**, 615-617 (1995).

12 Whittaker, C. A. & Hynes, R. O. Distribution and evolution of von Willebrand/integrin A domains: widely dispersed domains with roles in cell adhesion and elsewhere. *Molecular biology of the cell* **13**, 3369-3387, doi:10.1091/mbc.e02-05-0259 (2002).

13 Nielsen, H. V. *et al.* The Metal Ion-Dependent Adhesion Site Motif of the *Enterococcus faecalis* EbpA Pilin Mediates Pilus Function in Catheter-Associated Urinary Tract Infection. *mBio* **3**, e00177-00112, doi:10.1128/mBio.00177-12 (2012).

14 Flores-Mireles, A. L., Pinkner, J. S., Caparon, M. G. & Hultgren, S. J. EbpA vaccine antibodies block binding of *Enterococcus faecalis* to fibrinogen to prevent catheter-associated bladder infection in mice. *Science translational medicine* **6**, 254ra127-254ra127, doi:10.1126/scitranslmed.3009384 (2014).

15 Schembri, M. A., Lo, A. W. & Ulett, G. C. Blocking the 'MIDAS' touch of *Enterococcus faecalis*. *Annals of translational medicine* **3**, S3-S3, doi:10.3978/j.issn.2305-5839.2015.03.32 (2015).

16 Proft, T. & Baker, E. N. Pili in Gram-negative and Gram-positive bacteria - structure, assembly and their role in disease. *Cellular and molecular life sciences : CMLS* **66**, 613-635, doi:10.1007/s00018-008-8477-4 (2009).

17 Danne, C. & Dramsi, S. Pili of Gram-positive bacteria: roles in host colonization. *Research in Microbiology* **163**, 645-658, doi:https://doi.org/10.1016/j.resmic.2012.10.012 (2012).

18 Konto-Ghiorghi, Y. *et al.* Dual Role for Pilus in Adherence to Epithelial Cells and Biofilm Formation in *Streptococcus agalactiae*. *PLOS Pathogens* **5**, e1000422, doi:10.1371/journal.ppat.1000422 (2009).

19 Izore, T. *et al.* Structural basis of host cell recognition by the pilus adhesin from *Streptococcus pneumoniae*. *Structure (London, England : 1993)* **18**, 106-115, doi:10.1016/j.str.2009.10.019 (2010).

20 Becherelli, M. *et al.* The ancillary protein 1 of *Streptococcus pyogenes* FCT-1 pili mediates cell adhesion and biofilm formation through heterophilic as well as homophilic interactions. *Molecular microbiology* **83**, 1035-1047, doi:10.1111/j.1365-2958.2012.07987.x (2012).

21 Keogh, D. *et al.* Extracellular Electron Transfer Powers *Enterococcus faecalis* Biofilm Metabolism. *mBio* **9**, doi:10.1128/mBio.00626-17 (2018).

22 Shi, L. *et al.* Extracellular electron transfer mechanisms between microorganisms and minerals. *Nature reviews. Microbiology* **14**, 651-662, doi:10.1038/nrmicro.2016.93 (2016).

23 Weber, K. A., Achenbach, L. A. & Coates, J. D. Microorganisms pumping iron: anaerobic microbial iron oxidation and reduction. *Nature reviews. Microbiology* **4**, 752-764, doi:10.1038/nrmicro1490 (2006).

24 Sure, S. K., Ackland, L. M., Torriero, A. A., Adholeya, A. & Kochar, M. Microbial Nanowires: An Electrifying Tale. *Microbiology*, doi:10.1099/mic.0.000382 (2016).

25 Wang, F. *et al.* Structure of Microbial Nanowires Reveals Stacked Hemes that Transport Electrons over Micrometers. *Cell* **177**, 361-369.e310, doi:10.1016/j.cell.2019.03.029 (2019).

26 Light, S. H. *et al.* A flavin-based extracellular electron transfer mechanism in diverse Gram-positive bacteria. *Nature* **562**, 140-144, doi:10.1038/s41586-018-0498-z (2018).

27 Pankratova, G., Leech, D., Gorton, L. & Hederstedt, L. Extracellular Electron Transfer by the Gram-Positive Bacterium *Enterococcus faecalis*. *Biochemistry* **57**, 4597-4603, doi:10.1021/acs.biochem.8b00600 (2018).

28 Ramsey, M., Hartke, A. & Huycke, M. in *Enterococci: From Commensals to Leading Causes of Drug Resistant Infection* (eds M. S. Gilmore, D. B. Clewell, Y. Ike, & N. Shankar) (Massachusetts Eye and Ear Infirmary, 2014).

29 Sillanpaa, J. *et al.* Contribution of individual Ebp Pilus subunits of *Enterococcus faecalis* OG1RF to pilus biogenesis, biofilm formation and urinary tract infection. *PloS one* **8**, e68813, doi:10.1371/journal.pone.0068813 (2013).

30 Krishnan, V. *et al.* Structure of *Streptococcus agalactiae* tip pilin GBS104: a model for GBS pili assembly and host interactions. *Acta crystallographica. Section D, Biological crystallography* **69**, 1073-1089, doi:10.1107/S0907444913004642 (2013).

31 Shimaoka, M., Takagi, J. & Springer, T. A. Conformational regulation of integrin structure and function. *Annual review of biophysics and biomolecular structure* **31**, 485-516, doi:10.1146/annurev.biophys.31.101101.140922 (2002).

32 Kristich, C. J. *et al.* Development and use of an efficient system for random mariner transposon mutagenesis to identify novel genetic determinants of biofilm formation in the core *Enterococcus faecalis* genome. *Applied and environmental microbiology* **74**, 3377-3386, doi:10.1128/aem.02665-07 (2008).

33 Dale, J. L. *et al.* Comprehensive Functional Analysis of the *Enterococcus faecalis* Core Genome Using an Ordered, Sequence-Defined Collection of Insertional Mutations in Strain OG1RF. *mSystems* **3**, doi:10.1128/mSystems.00062-18 (2018).

34 Logan, B. E., Rossi, R., Ragab, A. a. & Saikaly, P. E. Electroactive microorganisms in bioelectrochemical systems. *Nature Reviews Microbiology*, doi:10.1038/s41579-019-0173-x (2019).

35 Logan, B. E. Exoelectrogenic bacteria that power microbial fuel cells. *Nature Reviews Microbiology* **7**, 375, doi:10.1038/nrmicro2113 (2009).

36 Rana, N. F. *et al.* Redox balance via lactate dehydrogenase is important for multiple stress resistance and virulence in *Enterococcus faecalis*. *Infection and immunity* **81**, 2662-2668, doi:10.1128/IAI.01299-12 (2013).

37 Huycke, M. M. *et al.* Extracellular superoxide production by *Enterococcus faecalis* requires demethylmenaquinone and is attenuated by functional terminal quinol oxidases. *Molecular microbiology* **42**, 729-740 (2001).

38 Vitreschak, A. G., Rodionov, D. A., Mironov, A. A. & Gelfand, M. S. Regulation of riboflavin biosynthesis and transport genes in bacteria by transcriptional and translational attenuation. *Nucleic acids research* **30**, 3141-3151 (2002).

39 Zhang, E., Cai, Y., Luo, Y. & Piao, Z. Riboflavin-shuttled extracellular electron transfer from *Enterococcus faecalis* to electrodes in microbial fuel cells. *Canadian journal of microbiology* **60**, 753-759, doi:10.1139/cjm-2014-0389 (2014).

40 Byappanahalli, M. N., Nevers, M. B., Korajkic, A., Staley, Z. R. & Harwood, V. J. Enterococci in the environment. *Microbiology and molecular biology reviews : MMBR* **76**, 685-706, doi:10.1128/MMBR.00023-12 (2012).

41 Benito, P. & Miller, D. Iron absorption and bioavailability: An updated review. *Nutrition Research* **18**, 581-603, doi:https://doi.org/10.1016/S0271-5317(98)00044-X (1998).

42 Saunders, S. H. & Newman, D. K. Extracellular Electron Transfer Transcends Microbe-Mineral Interactions. *Cell Host & Microbe* **24**, 611-613, doi:https://doi.org/10.1016/j.chom.2018.10.018 (2018).

43 Guiton, P. S. *et al.* Contribution of autolysin and Sortase a during *Enterococcus faecalis* DNA-dependent biofilm development. *Infection and immunity* **77**, 3626-3638, doi:10.1128/iai.00219-09 (2009).

44 Thomas, V. C., Thurlow, L. R., Boyle, D. & Hancock, L. E. Regulation of autolysis-dependent extracellular DNA release by *Enterococcus faecalis* extracellular proteases influences biofilm development. *Journal of bacteriology* **190**, 5690-5698, doi:10.1128/jb.00314-08 (2008).

45 Afonina, I., Lim, X. N., Tan, R. & Kline, K. A. Planktonic Interference and Biofilm Alliance between Aggregation Substance and Endocarditis- and Biofilm-Associated Pili in *Enterococcus faecalis*. *Journal of bacteriology* **200**, doi:10.1128/jb.00361-18 (2018).

46 Bourgogne, A., Thomson, L. C. & Murray, B. E. Bicarbonate enhances expression of the endocarditis and biofilm associated pilus locus, ebpR-ebpABC, in *Enterococcus faecalis*. *BMC Microbiol* **10**, 17, doi:10.1186/1471-2180-10-17 (2010).

47 Bourgogne, A. *et al.* EbpR is important for biofilm formation by activating expression of the endocarditis and biofilm-associated pilus operon (ebpABC) of *Enterococcus faecalis* OG1RF. *Journal of bacteriology* **189**, 6490-6493, doi:10.1128/JB.00594-07 (2007).

48 Manias, D. A. & Dunny, G. M. Expression of Adhesive Pili and the Collagen-Binding Adhesin Ace Is Activated by ArgR Family Transcription Factors in *Enterococcus faecalis*. *Journal of bacteriology* **200**, doi:10.1128/jb.00269-18 (2018).

49 Bourgogne, A., Hilsenbeck, S. G., Dunny, G. M. & Murray, B. E. Comparison of OG1RF and an Isogenic fsrB Deletion Mutant by Transcriptional Analysis: the Fsr System of *Enterococcus faecalis* Is More than the Activator of Gelatinase and Serine Protease. *Journal of bacteriology* **188**, 2875-2884, doi:10.1128/JB.188.8.2875-2884.2006 (2006).

50 Gao, P. *et al. Enterococcus faecalis* rnjB is required for pilin gene expression and biofilm formation. *Journal of bacteriology* **192**, 5489-5498, doi:10.1128/jb.00725-10 (2010).

51 Gao, P. *et al.* Functional studies of *E. faecalis* RNase J2 and its role in virulence and fitness. *PloS one* **12**, e0175212, doi:10.1371/journal.pone.0175212 (2017).

52 Glasauer, S., Langley, S. & Beveridge, T. J. Intracellular iron minerals in a dissimilatory iron-reducing bacterium. *Science (New York, N.Y.)* **295**, 117-119, doi:10.1126/science.1066577 (2002).

53 Ubeda, C. *et al.* Vancomycin-resistant *Enterococcus* domination of intestinal microbiota is enabled by antibiotic treatment in mice and precedes bloodstream invasion in humans. *The Journal of clinical investigation* **120**, 4332-4341, doi:10.1172/JCI43918 (2010).

54 Caballero, S. *et al.* Distinct but Spatially Overlapping Intestinal Niches for Vancomycin-Resistant *Enterococcus faecium* and Carbapenem-Resistant *Klebsiella pneumoniae*. *PLOS Pathogens* **11**, e1005132, doi:10.1371/journal.ppat.1005132 (2015).

55 Caballero, S. *et al.* Cooperating Commensals Restore Colonization Resistance to Vancomycin-Resistant *Enterococcus faecium*. *Cell Host Microbe* **21**, 592-602.e594, doi:10.1016/j.chom.2017.04.002 (2017).

56 La Rosa, S. L. *et al.* In vivo assessment of growth and virulence gene expression during commensal and pathogenic lifestyles of luxABCDE-tagged *Enterococcus faecalis* strains in murine gastrointestinal and intravenous infection models. *Applied and environmental microbiology* **79**, 3986-3997, doi:10.1128/aem.00831-13 (2013).

57 Riboulet, E. *et al.* Relationships between oxidative stress response and virulence in *Enterococcus faecalis*. *Journal of molecular microbiology and biotechnology* **13**, 140-146, doi:10.1159/000103605 (2007).

58 Aktan, Y., Tan, S. & Icgen, B. Characterization of lead-resistant river isolate *Enterococcus faecalis* and assessment of its multiple metal and antibiotic resistance. Vol. 185 (2012).

59 Colomer-Winter, C., Gaca, A. O. & Lemos, J. A. Association of Metal Homeostasis and (p)ppGpp Regulation in the Pathophysiology of *Enterococcus faecalis*. *Infection and immunity* **85**, doi:10.1128/iai.00260-17 (2017).

60 Karp, P. D. *et al.* The BioCyc collection of microbial genomes and metabolic pathways. *Briefings in bioinformatics*, doi:10.1093/bib/bbx085 (2017).

61 Kline, K. A. *et al.* Mechanism for Sortase Localization and the Role of Sortase Localization in Efficient Pilus Assembly in *Enterococcus faecalis. Journal of bacteriology* **191**, 3237-3247, doi:10.1128/jb.01837-08 (2009).

62 Waterhouse, A. *et al.* SWISS-MODEL: homology modelling of protein structures and complexes. *Nucleic Acids Res* **46**, W296-w303, doi:10.1093/nar/gky427 (2018).

63 Winn, M. D. *et al.* Overview of the CCP4 suite and current developments. *Acta Crystallogr D Biol Crystallogr* **67**, 235-242, doi:10.1107/s0907444910045749 (2011).

64 Emsley, P. & Cowtan, K. Coot: model-building tools for molecular graphics. *Acta Crystallogr D Biol Crystallogr* **60**, 2126-2132, doi:10.1107/s0907444904019158 (2004).

65 L DeLano, W. *The PyMOL Molecular Graphics System (2002) DeLano Scientific, Palo Alto, CA, USA.* http://www.pymol.org. (2002).

66 Banla, I. L. *et al.* Modulators of *Enterococcus faecalis* Cell Envelope Integrity and Antimicrobial Resistance Influence Stable Colonization of the Mammalian Gastrointestinal Tract. *Infection and immunity* **86**, e00381-00317, doi:10.1128/IAI.00381-17 (2017).

67 Zackular, J. P. *et al.* Dietary zinc alters the microbiota and decreases resistance to *Clostridium difficile infection*. *Nat Med* **22**, 1330-1334, doi:10.1038/nm.4174 (2016).

68 Juttukonda, L. J. *et al.* Dietary Manganese Promotes Staphylococcal Infection of the Heart. *Cell Host Microbe* **22**, 531-542.e538, doi:10.1016/j.chom.2017.08.009 (2017).

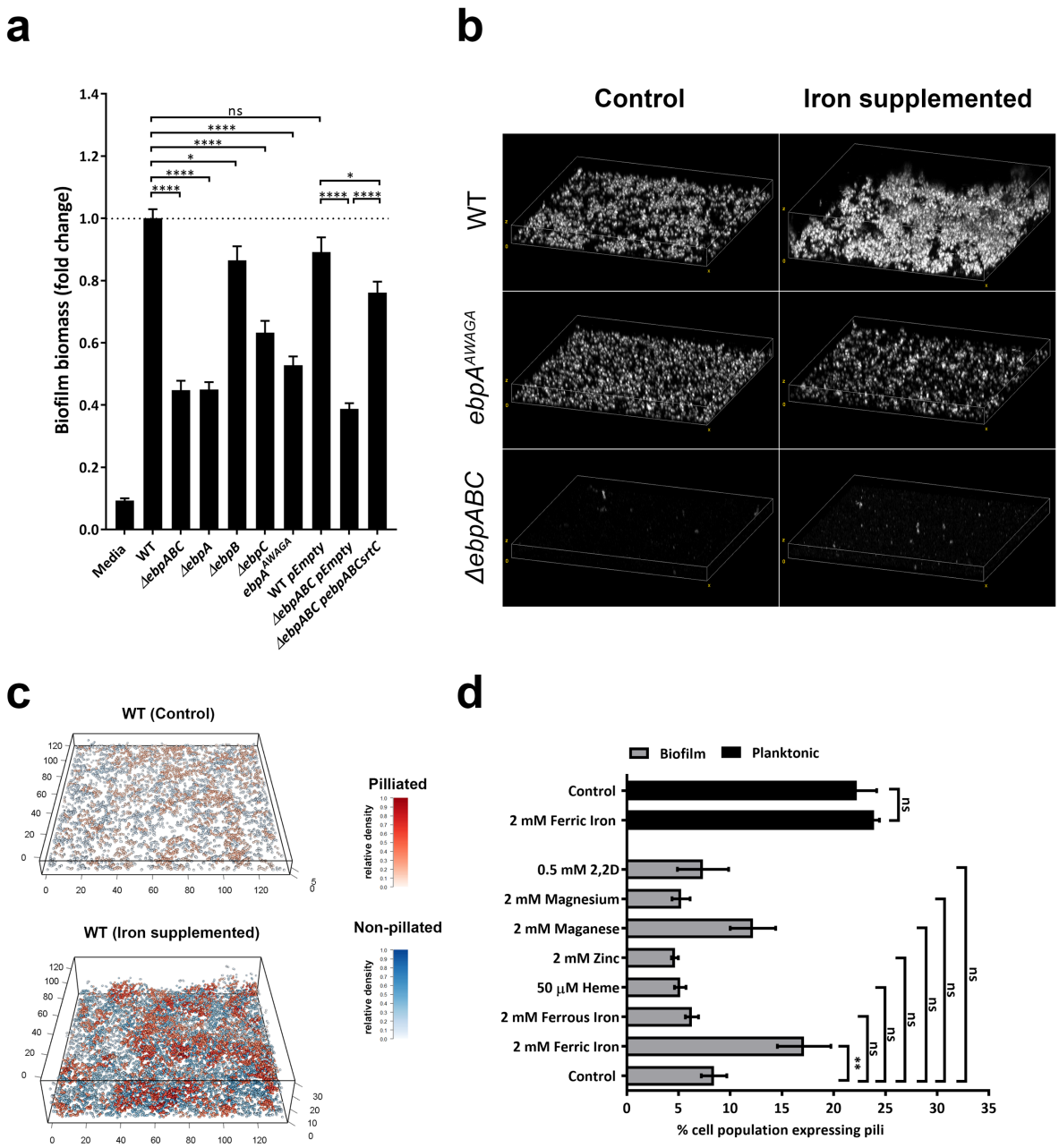

833

834 **Figure 1. Contribution of pilus to iron mediated *E. faecalis* biofilm growth. (a)** *E.*

835 *faecalis* biofilm biomass quantification grown for 120 hours using crystal violet staining.

836 N=9 repeated on non-consecutive days. **(b)** Volume viewer of CSLM images of *E. faecalis*

837 biofilm at 24 hr for control (40% TSBG) and iron-supplemented (40% TSBG, 0.2 mM $FeCl_3$)

838 at 63x magnification. *E. faecalis* cells are labeled with antibody against Group D antigen. **(c)**

839 Overlap of cell aggregation density map with the piliated cell population density map using

840 3D reconstruction of CLSM z-stack images of iron-supplemented *E. faecalis* biofilm

841 compared with control. N=3, repeated on non-consecutive days. **(d)** Quantification of
842 immuno-fluorescent labelled anti-EbpC *E. faecalis* cells from 6-well microtiter plate 24 hour
843 biofilm or planktonic culture grown at 37 ^{o}C in control and metal supplemented media. N>3.
844 Statistical significance was determined by two-way ANOVA. Error bars represent standard
845 error of the mean (SEM).
846
847
848
849
850
851
852
853
854
855
856
857
858
859
860
861
862
863
864
865

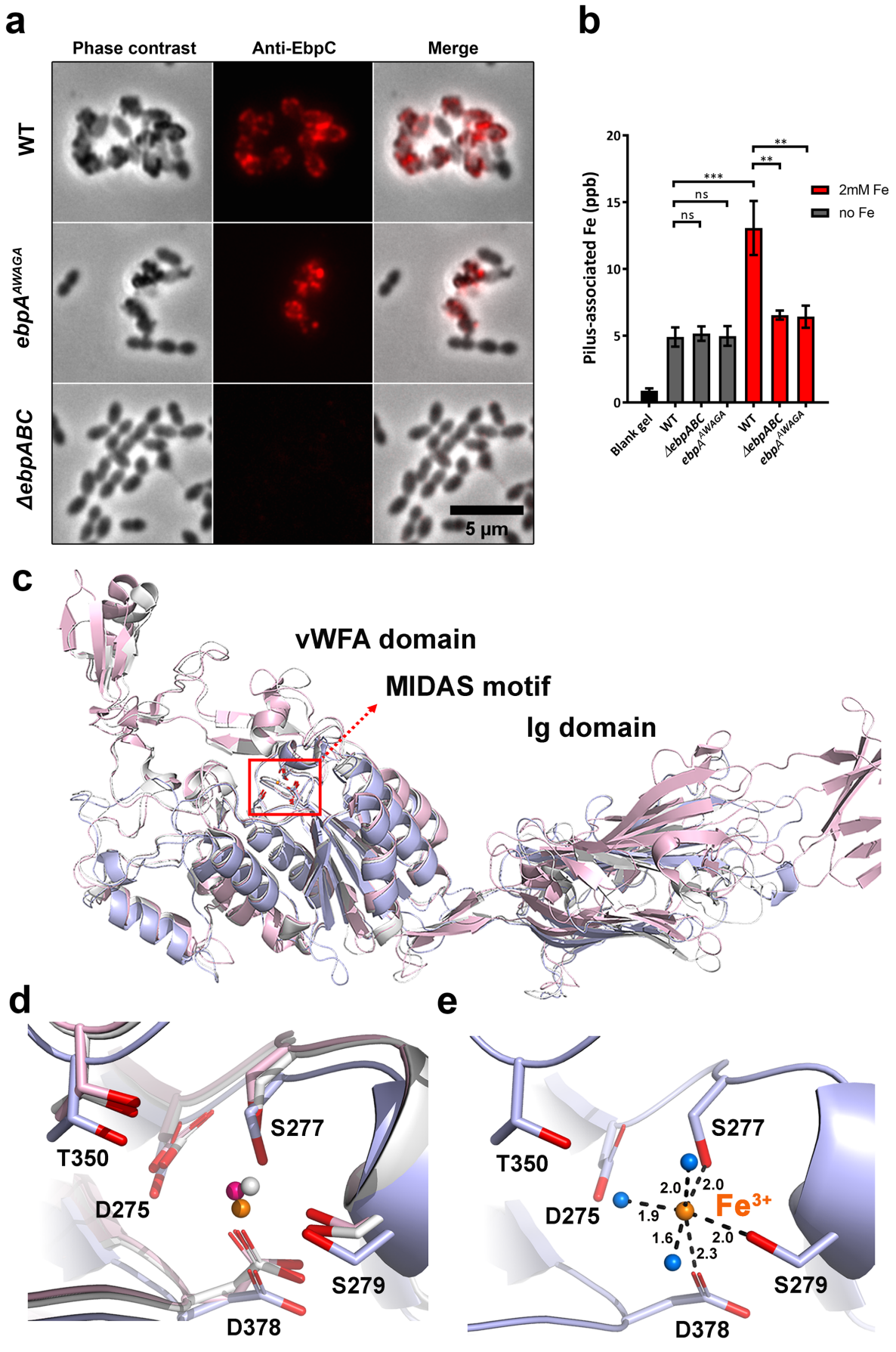

866

Figure 2. Evidences for EbpA-iron interaction. (a) Representative immunofluorescent images from 24 hour *E. faecalis* biofilm (wild type, Δ*ebpABC* and $ebpA^{AWAGA}$) labeled with EbpC antibody-conjugated fluorescent probe, grown from 6-well microtiter plate biofilm in the presence of iron, N=3. **(b)** ICP-MS analysis of iron (ppb) from pilus preps isolated under native condition. N=6. Statistical analysis is performed using two-way ANOVA Fisher LSD test. Error bars represent SEM. Black bar indicates 500nm. (**c**) Superimposition of EbpA structural model (N177-P620) (blue) with that of the *S. agalactiae* GBS104 (grey) and *S. pneumoniae* RrgA (pink). In agreement with other pilin adhesins, EbpA tip folds into a vWFA domain comprising of a 5 stranded β-sheet surrounded by 7 α-helices. The MIDAS motif is located at the N-terminus of the β-sheet. Only a partial model was obtained for the 2 extended arms of this domain. The EbpA tip is then followed by an IgG fold domain. (**d**) Closeup view of the superimposition of the MIDAS motif from EbpA (blue), GBS104 (grey) and RrgA (pink) showing conservation of D275, S277, S279, T350 and D378 residues (EbpA numbering). Bound Mg^{2+} ions (grey/magenta) in GBS104 and RrgA and modelled Fe^{3+}(orange) in EbpA are shown as spheres. (**e**) The Fe^{3+} is coordinated by the EbpA MIDAS motif by ~2Å direct interactions with S277, S279, D378 and a water mediated interaction with D275 along with interactions with two additional water molecules (water molecules shown as blue spheres). Upon a closed to open conformational change, bonding could shift from D378 to T350.

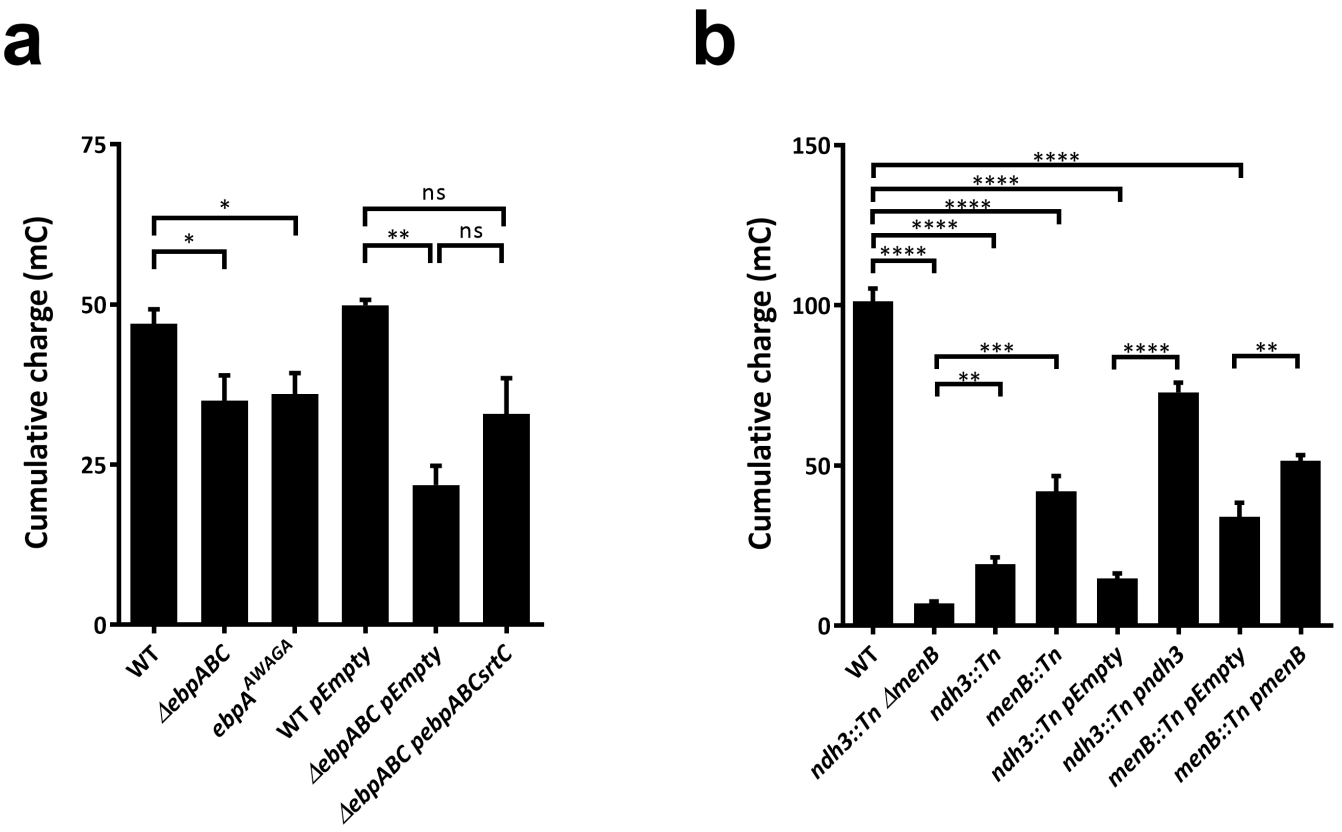

892

893 **Figure 3. Extracellular electron transfer in *E. faecalis* biofilm. (a)** Cumulative charge production (over 20 hours) in *E. faecalis* pilin mutants
894 grown in the presence of 0.5 mM iron and **(b)** EET-associated mutants grown in the presence of 2 mM iron on a screen-printed carbon mini-
895 electrode for 20 hours in a closed static system at 37^{o}C. Experiments were repeated on non-consecutive days, N>3. Statistical analysis is
896 performed using one-way ANOVA with Bonferroni multiple comparison test. Error bar represents standard error margin (SEM).

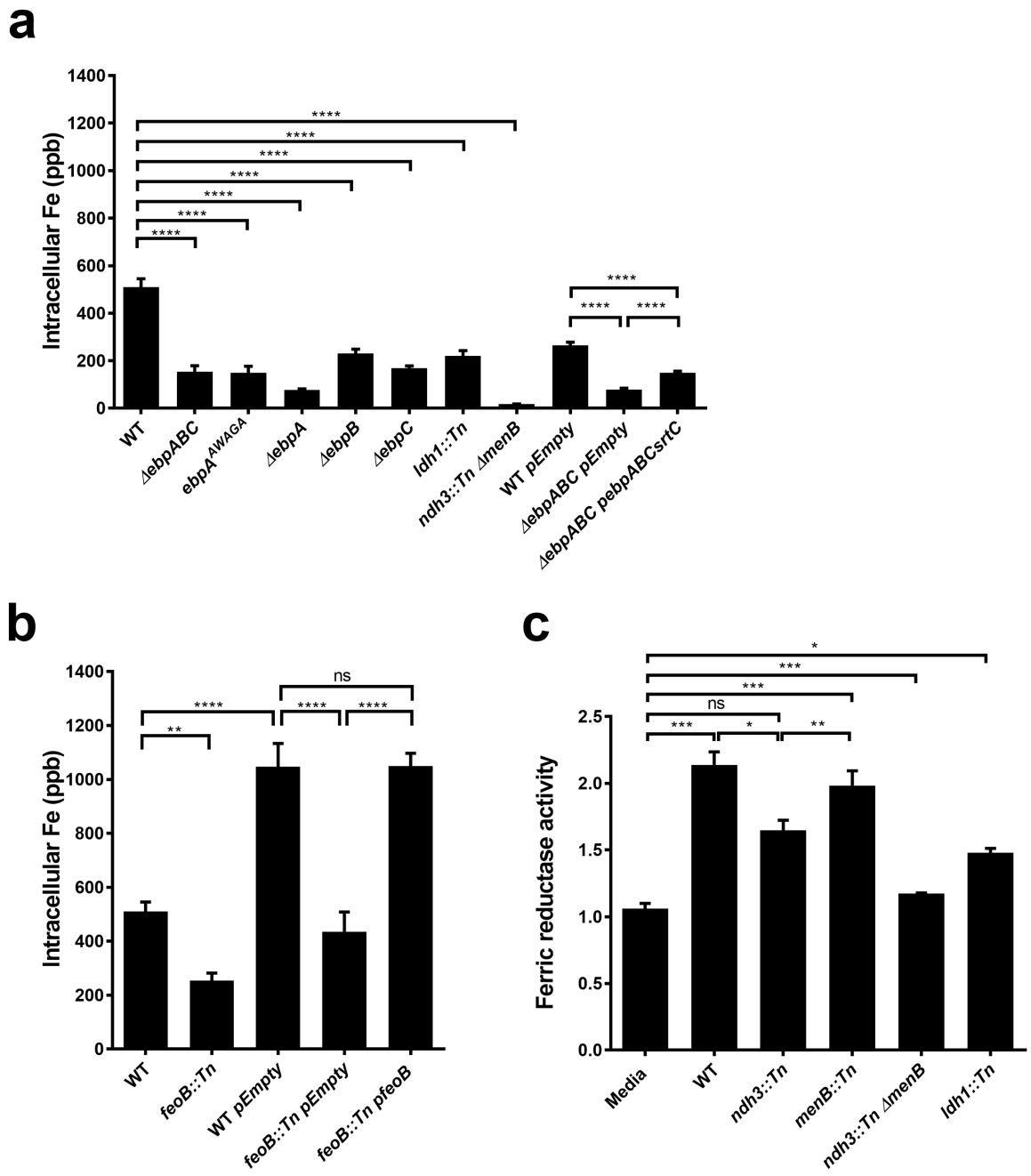

Figure 4: Intracellular iron accumulation is dependent on the ability for extracellular ferric iron reduction. (a-b) ICP-MS analysis of intracellular iron (ppb) in *E. faecalis* biofilm cells grown in iron-supplemented media. N=9. **(c)** Quantification of ferric iron reduction activity by *E. faecalis*. Statistical significance was determined by one-way ANOVA. Error bars represent standard error margin (SEM).

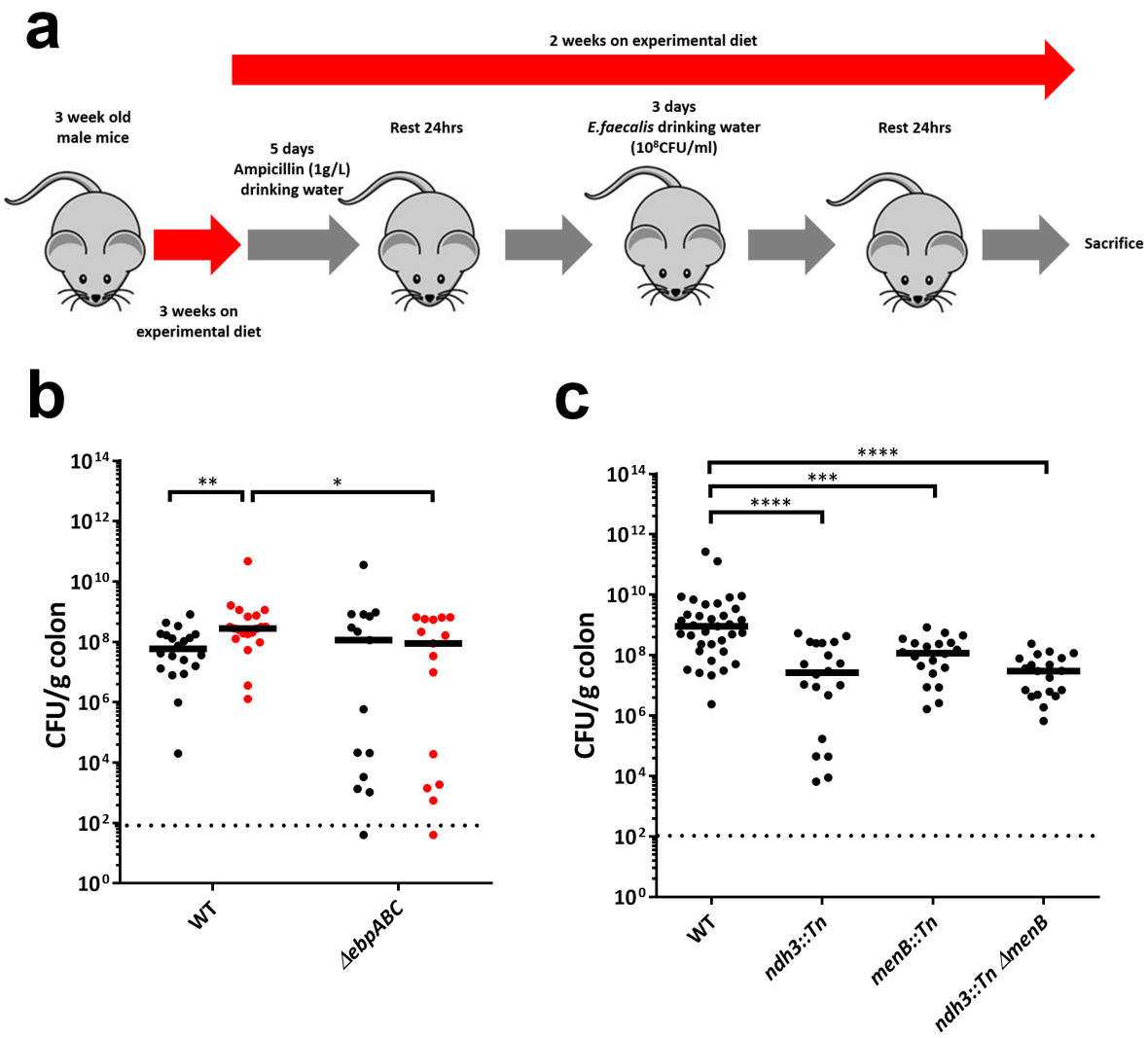

Figure 5. *E. faecalis* colonization in lower gastrointestinal tract. (a) Schematic of diet manipulation in GI colonization model. **(b)** Bacterial titers of pilus null mutant (N=3, n=5) and EET-associated mutants (for WT n=30, for mutants n=15) recovered from mouse colons, repeated on non-consecutive days. Statistical significance was determined by Mann-Whitney test. Black line indicates the median. Dotted line indicates limitation of detection at CFU <40.

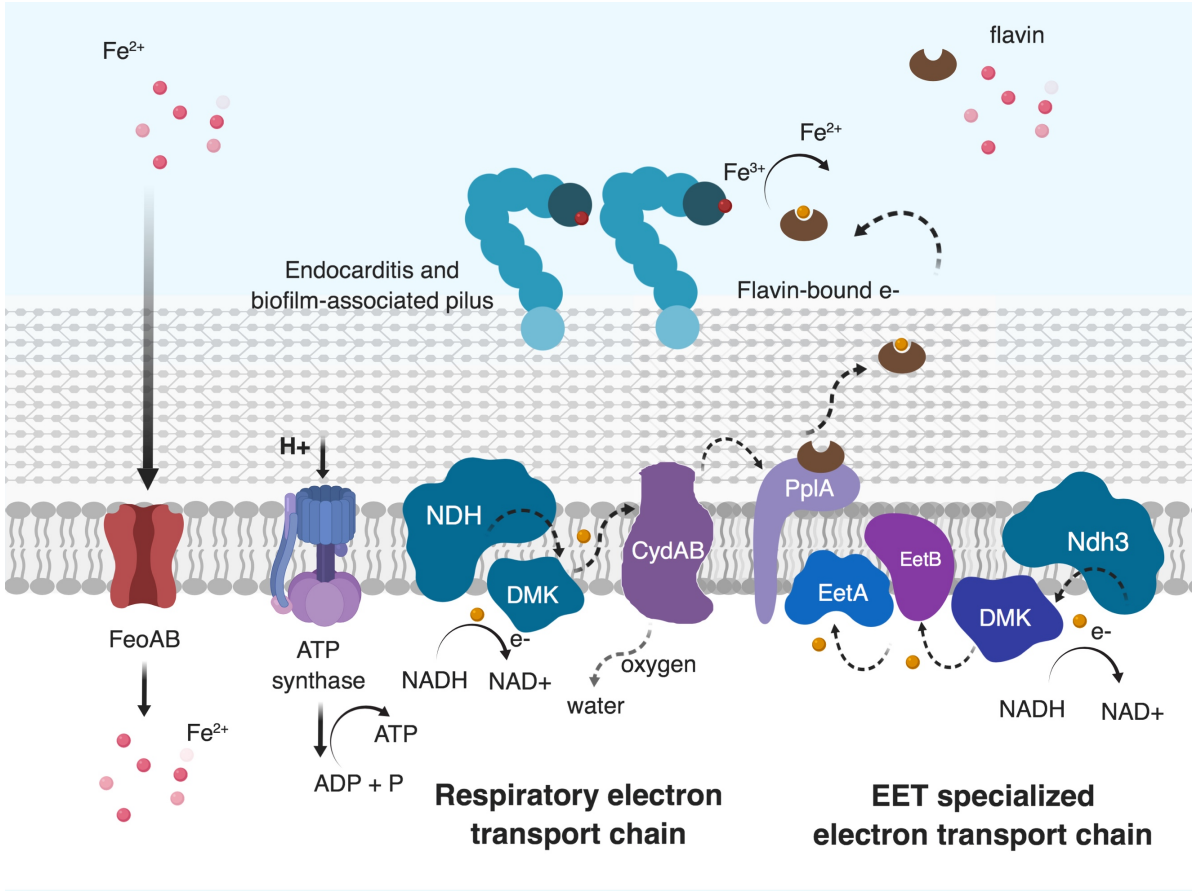

914

915 **Figure 6. Model for the role of iron in *E. faecalis* biofilm.** Biofilm growth in excess iron induces expression of the genes encoding the sortase-
916 assembled Ebp, which in turn associate with iron via the MIDAS motif of the EbpA tip adhesin. EET is dependent on both DMK in the electron
917 transport chain, as well as a specialized flavin-associated respiratory chain, leading to reduction of extracellular iron and FeoB-mediated uptake
918 of reduced free ferrous iron.

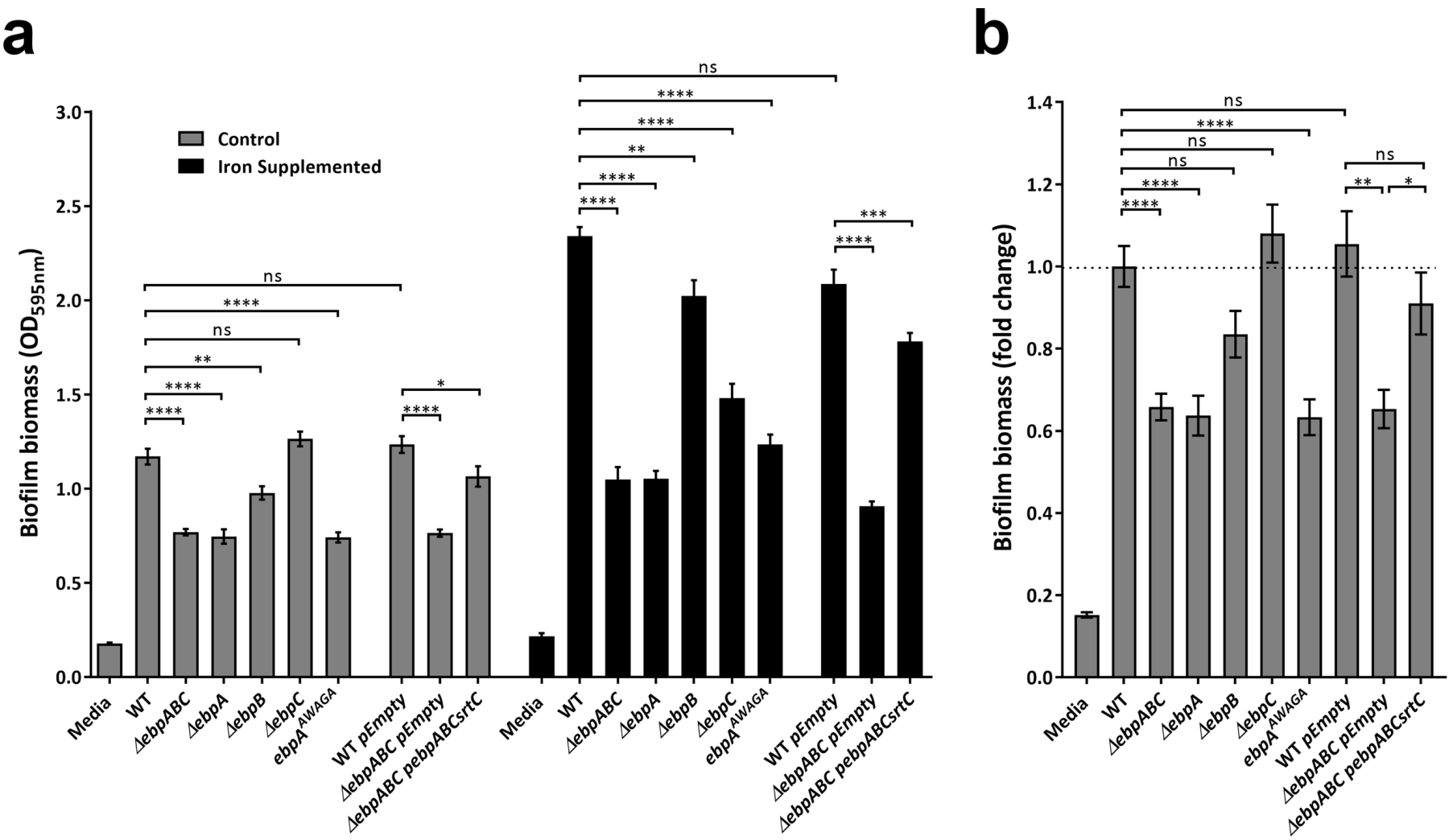

Figure S1. Pili contribution to biofilm formation. (a) *E. faecalis* biofilm total biomass quantification and **(b)** fold change calculations for the same data shown in Fig 1A and Fig S1A after growth for 120 hours grown in non-supplemented and iron-supplemented media in 96-well

922 microtiter plate as measured by crystal violet staining. N=9 repeated on non-consecutive days. Statistical significance was determined by two-
923 way ANOVA. Error bars represent the standard error of the mean (SEM).
924
925
926
927
928
929
930
931
932
933
934
935
936
937
938

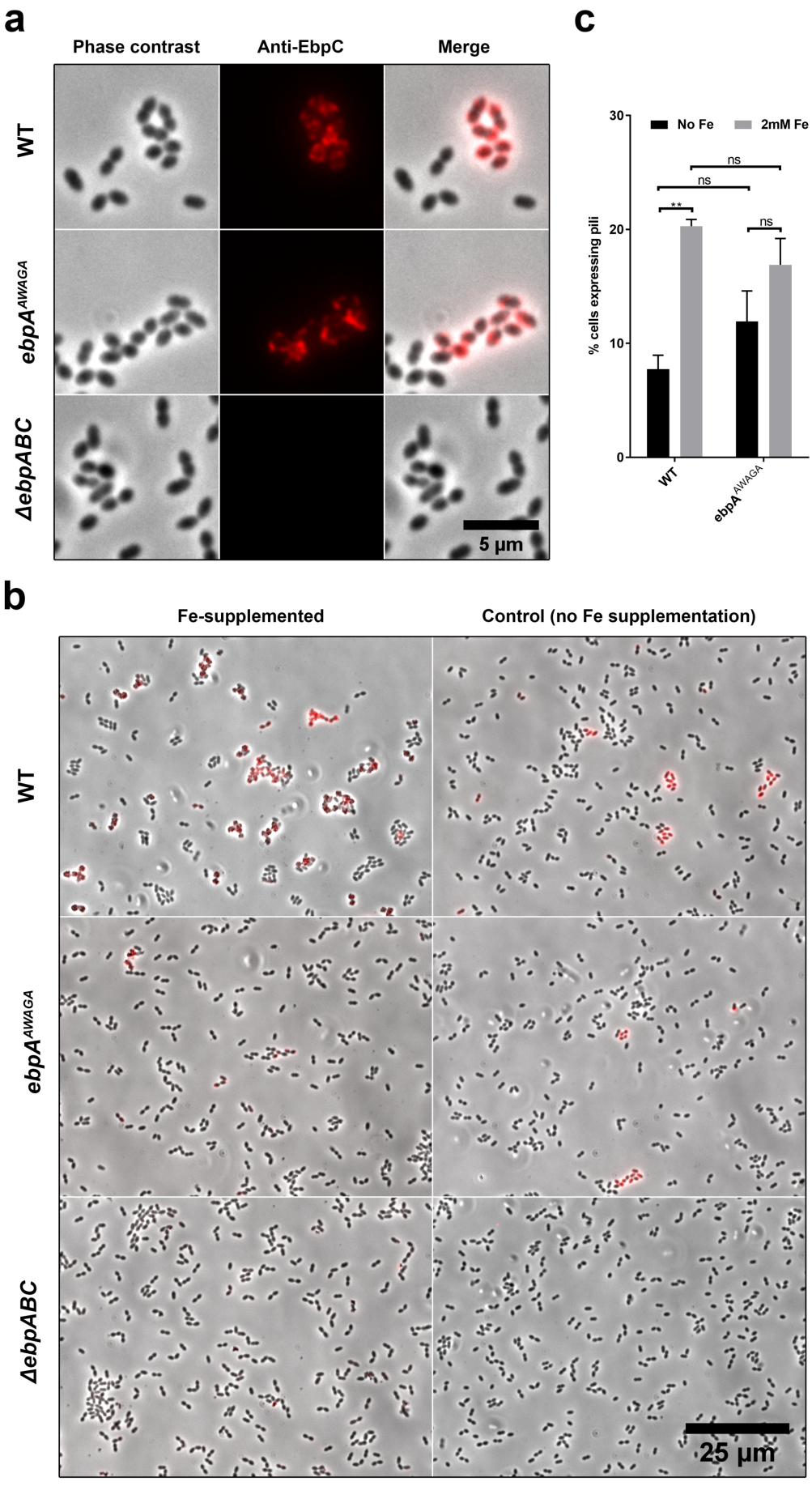

939

Figure S2. Antibody specificity against cell surface expressed pili. Representative immunofluorescent images of *E. faecalis* and pilus mutants **(a)** cropped and **(b)** at original 63x magnification from biofilm grown in 6-well microtiter plates for 24 hours at 37 degrees in non-supplemented media or both non-supplemented and iron-supplemented media. N=6, with 5 images per biological replicate, capturing approximately 100-300 cells per images, repeated on non-consecutive days. **(c)** Quantification of immuno-fluorescent labelled anti-EbpC *E. faecalis* cells from 6-well microtiter plate 24hr biofilm grown at 37 degrees in control and metal supplemented media. Statistical significance was determined by two-way ANOVA with Bonferroni multiple comparison test. Error bars represent the standard error of the mean (SEM).

```
EbpA      MITDENDKTNINIELNLLNQTEQPLQREIQLKNAQFMDTAVIEKDGYSYQVTNGTLYLTL   60
GBS104    ------------------------------MKKRQKIWRGLSVTLLILSQI---P--FGI   25
RrgA      ------------------------MLNRETHMKKVRKIFQKAVAGLCCISQL---TAFSSI   34
                                       :*: : :            *:        :

EbpA      DAQVK----KPVQLSLAVEQSSLQTAQPPKLLYE-NNEYDVSVTSEKITVEDS---AKES   112
GBS104    LVQGETQDTNQALGKVIVKKTGDNATPLGKATFVLKNDNDKSETSHE-TVEGSGEATFEN   84
RrgA      VALAETPETSPAIGKVVIKETGEGGALLGDAVFELKNNTDGTTVSQR-TEAQTGEAIFSN   93
           .  :    . .  .: ::::.   :   .  :  :*: * : .*.. *   :     ..

EbpA      TEPEKITVPENTK-----ETNKNDSAPEKTEQPTATEEVTNPFAEARMAPATLRANLALP   167
GBS104    IKPGDYTLREETAPIGYKKTDKTWKVKVADNGATIIEGMDADKAE-----------KRKE   133
RrgA      IKPGTYTLTEAQPPVGYKPSTKQWTVEVEKNGRTTVQGE---QVE-----------NREE   139
           :*   *: *         : *  ..    :  *  :      .*

EbpA      LIAPQYTTDNSGTYPTANWQPTGNQNVLNHQGNKDGGAQWDGQTSWNGDPTNRTNSYTEY   227
GBS104    VLNAQYP--KSAIYEDTK----ENYPLVNVEGSKVG-EQYKALNPINGKDGRREIAE---   183
RrgA      ALSDQYP--QTGTYPDVQ----TPYQIIKVDGSEKN-GQHKALNPN---PYERVIPE---   186
           :  **   ::. *  .:        ::: :*.: .  * .. .       .*

EbpA      GGTGDQADYAIRKYARETTTPGLFDVYLNVRGNV----QKEITPLDLVLVVDWSGSMNEN   283
GBS104    -G-----WLSKKITGVNDLDKNKYKIELTVEGKTTVETKELNQPLDVVVLLDNSNSMNNE   237
RrgA      -G-----TLSKRIYQVNNLDDNQYGIELTVSGKTVYEQKDKSVPLDVVILLDNSNSMSNI   240
           *       : :    :    . : : *.* *:.    :.   ***:*:::* *.**.:

EbpA      NRIG-----EVQKGVNRFVDTLADSGITNNINMGYVGYSSDGYN----------------   322
GBS104    RANNSQRALKAGEAVEKLIDKITSNKD---NRVALVTYASTIFDGTEATVSKGVADQNGK   294
RrgA      RNKNARRAERAGEATRSLIDKITSDSE---NRVALVTYASTIFDGTEFTVEKGVADKNGK   297
           .  .     .. :... ::*.::..      .:. * *:*  ::

EbpA      ----------------NNAIQM---------GPFDTVKN-------PIKNITPSSTRGGT   350
```

```
998   GBS104    ALNDSVSWDYHKTTFTATTHNYSYLNLTNDANEVNILKSRIPKEAEHINGDRTLYQFGAT  354
999   RrgA      RLNDSLFWNYDQTSFTTNTKDYSYLKLTNDKNDIVELKNKVPTEAEDHDGNRLMYQFGAT  357
1000                          .: :          . .  :*.         ..       *.*
1001
1002  EbpA      FTQKALRDAGDMLATP--NGHKKVIVLLTDGVPTFSYKVSRVQTEADGRFYGTQFTNRQD  408
1003  GBS104    FTQKALMKANEILETQSSNARKKLIFHVTDGVPTMSYAINFNPY-ISTS-YQNQFN----  408
1004  RrgA      FTQKALMKADEILTQQARQNSQKVIFHITDGVPTMSYPINFNHATFAPS-YQNQLN----  412
1005              ****** .*.::*     :  :*:*. :******:** :.          * .*:.
1006
1007  EbpA      QPGSTSYISGSYNAPDQNNISKRINSTFIATI--GEAMALKQRGIEIHGLGIQLQSDPRA  466
1008  GBS104    -----SFLN---KIPDRSGI---LQEDFIING--DDYQIVKGD-----GESFKLFSD---  447
1009  RrgA      -----AFFS---KSPNKDGI---LLSDFITQATSGEHTIVRGD-----GQSYQMFTD---  453
1010                ::::.   : *::..*   : . **     .:   ::       * . :: :*
1011
1012  EbpA      NLSKQQVEDKMREMVSADENGDLYYESADYAPDISDYLAKKAVQISGTVVNGKVVDPIAE  526
1013  GBS104    ----------------------------------------RKVPVTGG--------TTQA  459
1014  RrgA      ----------------------------------------KTVYEKGA--------P--A  463
1015                                                   : *  .*
1016
1017  EbpA      PFKYEPNTLSMKSVGPVQVQTLPEVSLTGATINSNEIYLGKGQEIQIHYQVRIQT-----  581
1018  GBS104    AYRVPQNQLSVMS--------NEGY-----AINSGYIYLYWRDYN-WVYPFDPKTKKVSA  505
1019  RrgA      AFPVKPEKYSEMK--------AAGYAVIGDPINGGYIWLNWRESI-LAYPFNSNTA----  510
1020               :    :  *  .                 **.. *:*   :     * .  :*
1021
1022  EbpA      ---ESENFKPDFWYQMNGRTTFQPLATAPEKVDFGVPSGKAPGVKLNVKKIWEEYDQDPT  638
1023  GBS104    TKQIKTHGEPTTLYFNGN-I--RPKGYDI--FTVGIGVNGDPGATPLE---AEKFMQSIS  557
1024  RrgA      --KITNHGDPTRWYYNGN-I--APDGYDV--FTVGIGINGDPGTDEAT---ATSFMQSIS  560
1025              . : .*   *  ..     * .     . .*:  .  **.         .: *. :
1026
1027  EbpA      SRPDNVIYEISRKQVTDTANWQTGYIKLSKPENDTSNSWERKNVTQLSKTADESYQEVLG  698
1028  GBS104    SKTEN----------------------------YTNVDDTNKIYDELNKY----FKTIVE  585
1029  RrgA      SKPEN----------------------------YTNVTDTTKILEQLNRY----FHTIVT  588
```

```
1030                *: :*                            *.     *   :*.:     :: ::
1031
1032  EbpA          LPQYNNQGQAFNYQTTRELAVPGYS---QEKIDDTTWKNTKQFKPLDLKVIKNSSSGEKN    755
1033  GBS104        ---------------EKHSIVDGNVTDPMGEMIEFQLKNGQSFTHDDYVLVGNDGSQLKN    630
1034  RrgA          ---------------EKKSIENGTITDPMGELIDLQLGTDGRFDPADYTLTANDGSRLEN    633
1035                               :.    *       :: :    .   *   *  :  *..*  :*
1036
1037  EbpA          LVGAVFELSGKNVQTTLVDNKDGSYSLPKDVRLQKGERYTLTEVKAPAGHELGKKTTWQI    815
1038  GBS104        GV----ALGGPNSDGGILKDVTVTYD---------------------------------    652
1039  RrgA          GQ----AVGGPQNDGGLLKNAKVLYD---------------------------------    655
1040                      :.* : :  ::.:    *.
1041
1042  EbpA          EVNEQGKVSIDGQEVTTTNQVIPLEIENKFSSLPIRIRKYTMQNGKQVNLAEATFALQRK    875
1043  GBS104        ----------------------------KTSQTIKINHLNLGSGQKVVLTY---DVRLK    680
1044  RrgA          ----------------------------TTEKRIRVTGLYLGTDEKVTLTY---NVRLN    683
1045                                           :.  *::    : ..::* *:     :: :
1046
1047  EbpA          NA---QGSYQTVATQKTDTAGLSYFKISEPGEYRMVEQSGPLGYDTLAGNYEFTVDKYGE    932
1048  GBS104        DNYISNKFYNTNNR-----TTLSPKSEKEPNTI-----------------RDFPIPKIR-    717
1049  RrgA          DEFVSNKFYDTNGR-----TTLHPKE-VEQNTV-----------------RDFPIPKIR-    719
1050                :    :  *:*        : *   .  * .                   :* : *
1051
1052  EbpA          IHYAGKNIEENAPEWTLTHQNHLKPFDLTVHKKADNQTPLKGAKFRLTGPDTDIEL----    988
1053  GBS104        -------DVREFPVLTISNQKKMGEVEFIKVNKDKHSESLLGAKFQLQIEK-DF---SGY    766
1054  RrgA          -------DVRKYPEITISKEKKLGDIEFIKVNKNDK-KPLRGAVFSLQKQHPDYPDIYGA    771
1055                         .: *  *:::::::  .::   :* .:   * ** * *   . *
1056
1057  EbpA          --------PKDGKETDTFVFENLKPGKYVLTETFTPEGYQGLKEPIE-LIIREDGSVTID    1039
1058  GBS104        KQFVPEGSDVTTKNDGKIYFKALQDGNYKLYEISSPDGYIEVKTKPVVTFTIQNGEVTNL    826
1059  RrgA          IDQNGTYQNVRTGEDGKLTFKNLSDGKYRLFENSEPAGYKPVQNKPIVAFQIVNGEVRDV    831
1060                             : ..: *: *. *:* * *   * **  ::      :   :*.*
1061
```

```
EbpA        GEKV-AD----VLISGEKNNQITLDVTNQAKVPLPETGGIGRLWFYLIAISTFVIAGVYL    1094
GBS104      KADPNANKNQIGYLEGNG-KHLITNTPKRPPGVFPKTGGIGTIVYILVGSTFM-ILTICS    884
RrgA        TSIV-PQDIPAGYEFTND-KHYITNEPIPPKREYPRTGGIGMLPFYLIGCMMM-GGVLLY    888
                      :         :  ::   :         *.***** : : *:.   :    :

EbpA        FIRRPEGSV    1103
GBS104      FRRKQL---    890
RrgA        TRKHP----    893
              ::
```

Figure S3. Clustal alignment of EbpA homologs

Alignment of the EbpA sequence with *S. agalactiae* GBS104 (Q8E0S5) and *S. pneumoniae* RrgA (A0A0H2UNT6), showing conservation of the EbpA MIDAS motif and associated metal binding residues.

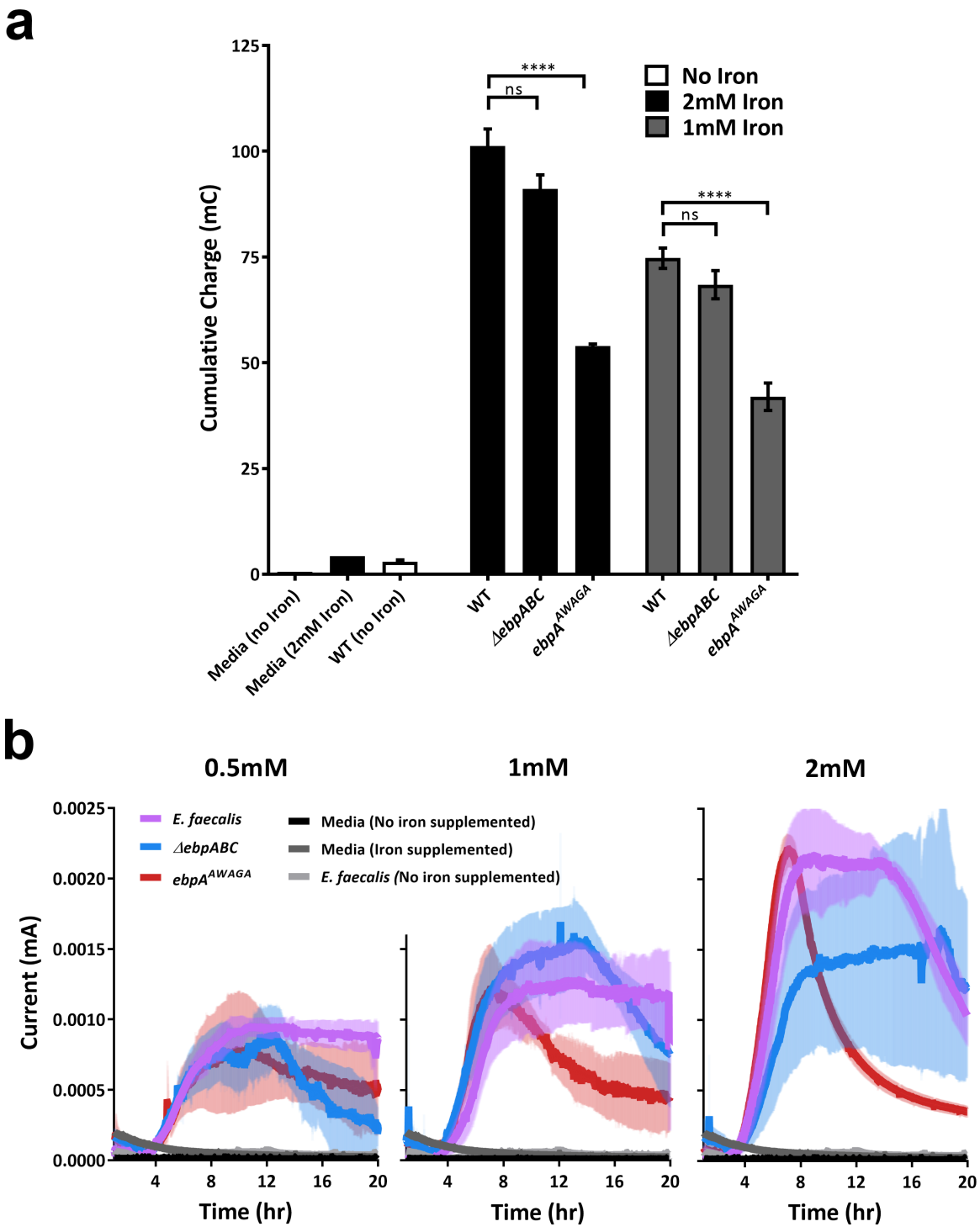

Figure S4. Current output and cumulative charge production of pilin mutants in a dosage dependent manner. (a) Cumulative charge production over 20 hours and **(b)** current output in *E. faecalis* mutants grown on a screen-printed carbon mini-electrode over 20 hr in closed static system at 37°C at 0.5 mM, 1 mM and 2 mM iron concentrations. Statistical

analysis is performed using one-way ANOVA with Bonferroni multiple comparison test, N>3. Error bars represent the standard error of the mean (SEM).

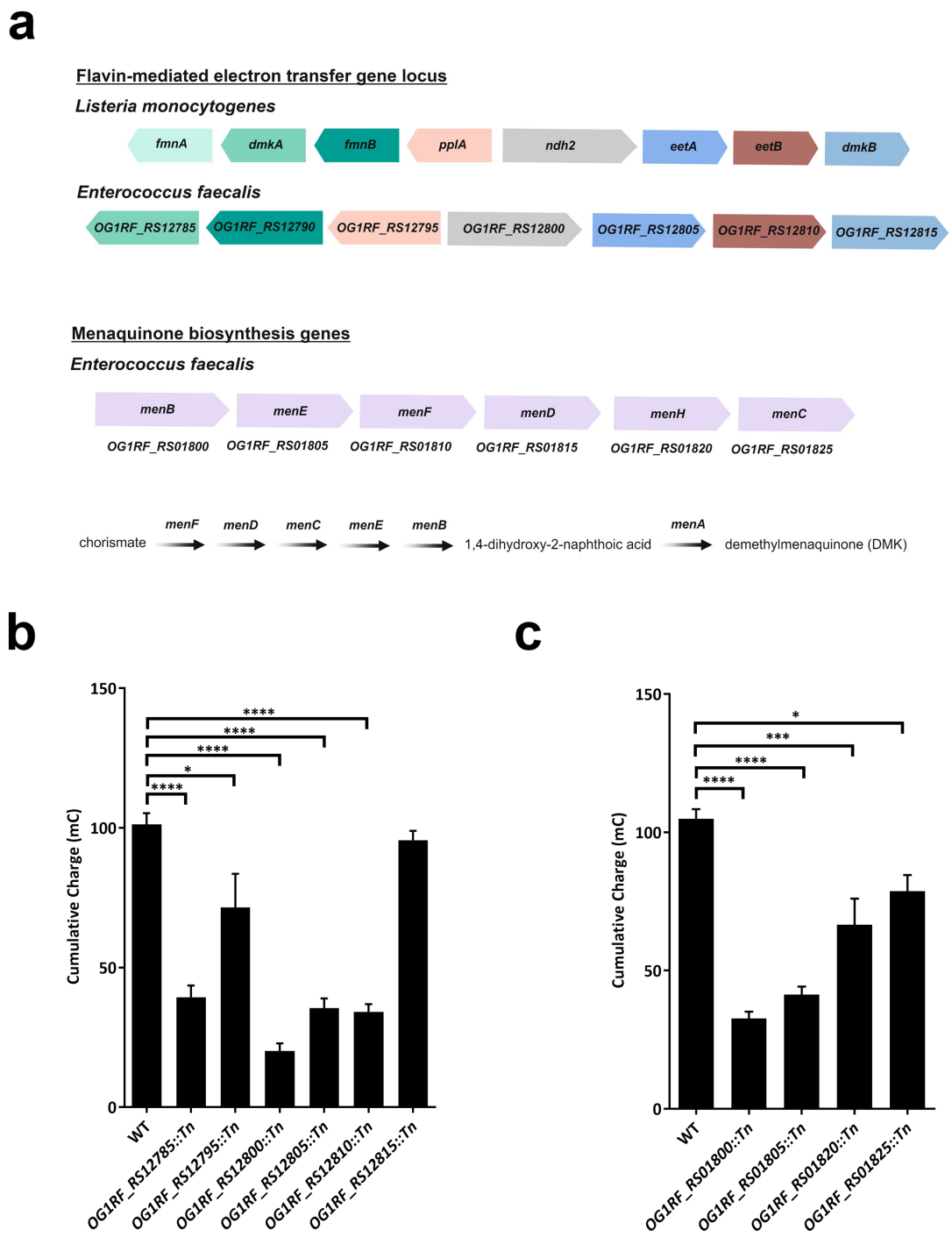

Figure S5. Respiratory electron transport mechanisms in *E. faecalis*. (a) Gene homologs of EET specialized respiratory electron transport chain and menaquinone biosynthesis genes required for DMK. **(b)** Cumulative charge production over 20 hours by *E. faecalis* mutants of EET specialized gene locus and menaquinone biosynthesis genes grown on a screen-printed carbon mini-electrode over 20 hr in closed static system at 37^{o}C at 2 mM iron concentration,

N=3. Statistical analysis is performed using one-way ANOVA with Bonferroni multiple comparison test. Error bars represent the standard error of the mean (SEM).

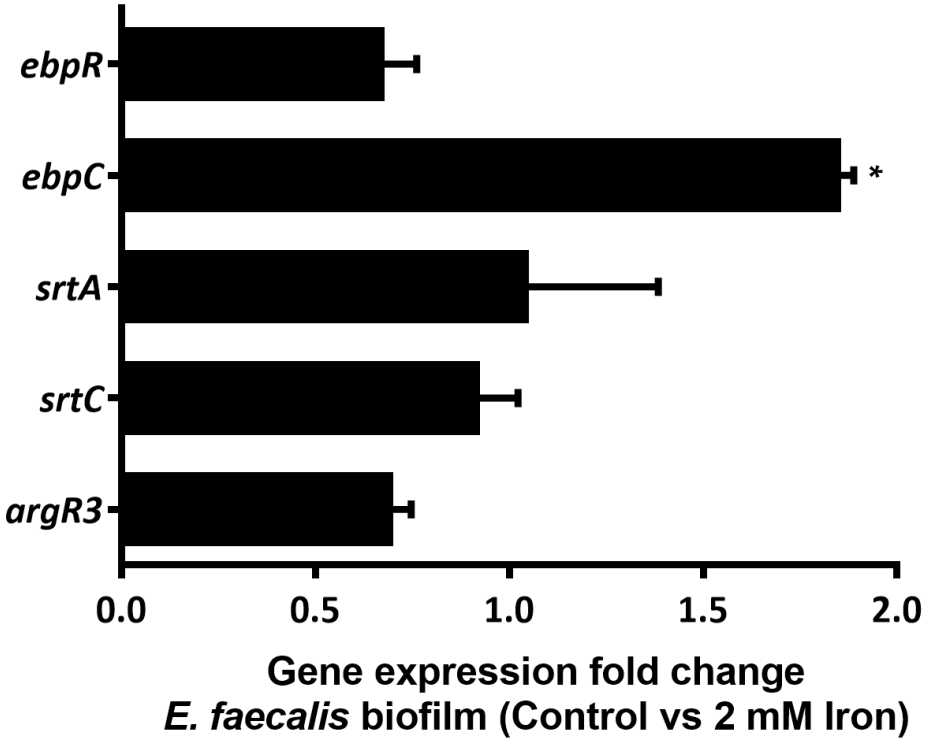

Figure S6. Regulation of pilus-associated genes in response to iron. qRT-PCR of RNA transcript abundance of genes associated with pilus biogenesis. N=6, repeated on non-consecutive days. N=9. Statistical significance was determined by one-way ANOVA. Error bars represent the SEM.

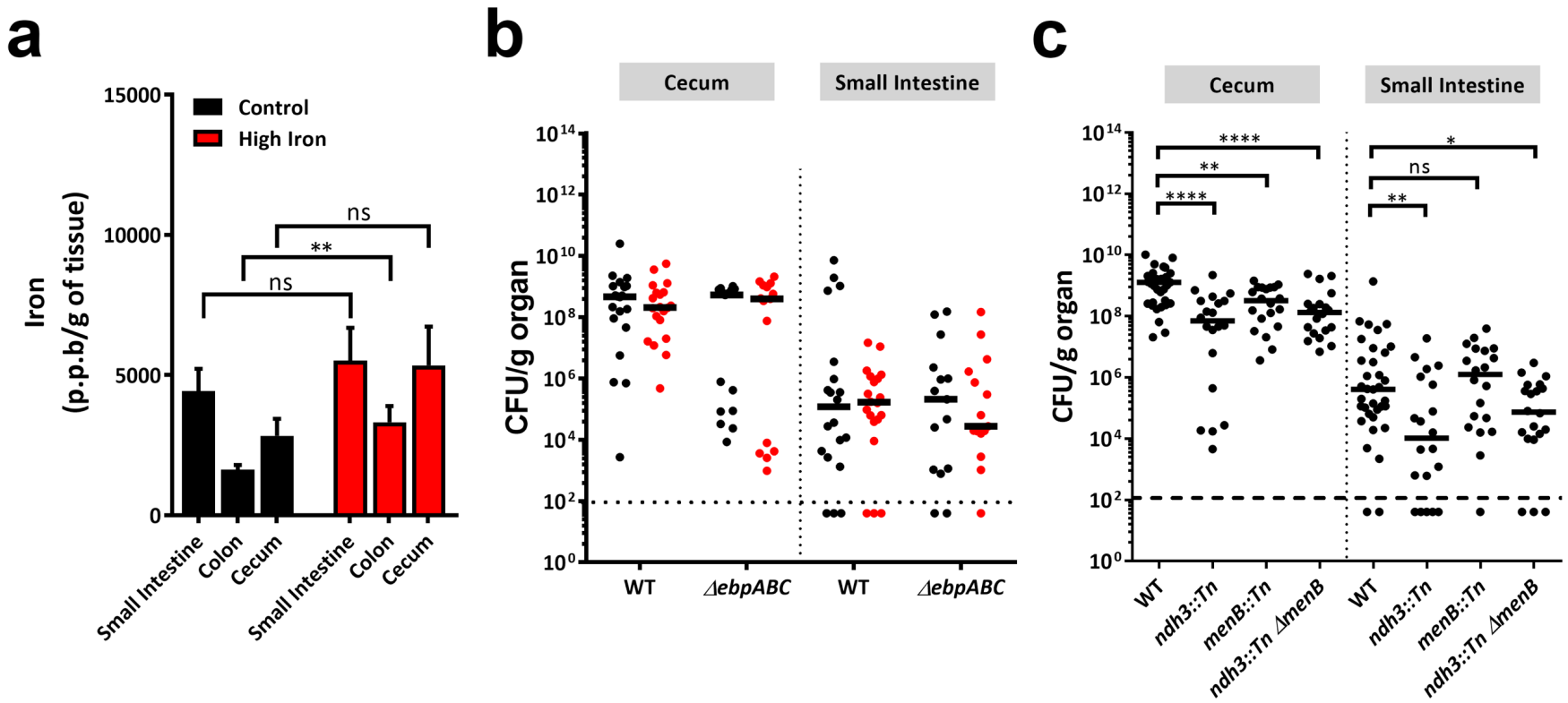

Figure S7. *E. faecalis* pilin mutant colonization in mouse lower gastrointestinal tract. (a) ICP-MS analysis of iron in the mouse tissues after feeding on normal or high iron diets, N=2, n=5. **(b)** Bacterial titers of pilin mutants recovered from the mouse cecum and small intestine, N=3, n=5. **(c)** Bacterial titers of EET associated mutants recovered from the mouse cecum and small intestine, N=3, n=5. Statistical significance was determined by Mann-Whitney test. Black line indicates median. Dotted line indicates limitation of detection of CFU <40.

Supplementary Table 1. RNA-sequencing results.

Old Gene Locus	New Gene Locus	RF-Bio1	RF-Bio2	RF-Bio3	RF_Fe-Bio1	RF_Fe-Bio2	RF_Fe-Bio3	logFC	logCPM	P-Value	FDR	Annotation
OG1RF_10072	OG1RF_RS00365	8511.8527	6488.9180	7624.4051	2705.9691	2800.5727	3142.9526	-1.3872	12.3487	0.0003	0.0140	transcriptional regulator (stress response regulator Gls24)
OG1RF_10073	OG1RF_RS00370	3214.8225	2303.0033	4763.1714	1013.7927	1268.0472	1233.1796	-1.5480	11.1690	0.0002	0.0111	membrane protein (transglycosylase associated protein)
OG1RF_10171	OG1RF_RS00860	1352.7718	926.4525	639.5307	3502.8808	2184.6641	2369.1118	1.4632	10.8424	0.0007	0.0268	preprotein translocase subunit SecY
OG1RF_10172	OG1RF_RS00865	411.1365	292.5639	283.1256	1160.0613	713.7294	798.6700	1.4329	9.2682	0.0005	0.0212	adenylate kinase
OG1RF_10269	OG1RF_RS01485	79.5748	82.5180	73.2796	161.3998	173.9036	240.0148	1.2876	7.1469	0.0017	0.0468	esterase
OG1RF_10296	OG1RF_RS01630	10.6100	18.7541	19.9853	65.5687	68.8368	64.1419	2.0227	5.5802	0.0001	0.0046	PTS mannitol transporter subunit IICB
OG1RF_10338	OG1RF_RS01840	1249.3246	465.1016	886.0165	254.7091	396.7176	326.9167	-1.4098	9.2303	0.0019	0.0500	osmotically inducible protein C
OG1RF_10340	OG1RF_RS01850	29.1774	7.5016	13.3236	113.4843	54.3449	78.6255	2.2048	5.8090	0.0000	0.0036	PTS sorbose transporter subunit IIC
OG1RF_10360	OG1RF_RS01950	172.4121	97.5213	109.9193	393.4121	226.4370	380.7132	1.3840	7.8873	0.0014	0.0405	ferrous iron transport protein B
OG1RF_10396	OG1RF_RS02135	1726.7735	1425.3115	1122.5096	522.0276	280.7819	403.4732	-1.8269	9.8397	0.0000	0.0017	hypothetical protein
OG1RF_10541	OG1RF_RS02845	198.9370	225.0492	369.7287	65.5687	94.1978	120.0074	-1.4948	7.5083	0.0007	0.0268	membrane protein (transglycosylase-associated protein)
OG1RF_10544	OG1RF_RS02860	140.5822	56.2623	99.9267	494.2870	278.9704	289.6731	1.8213	7.8679	0.0001	0.0057	glucuronyl hydrolase
OG1RF_10545	OG1RF_RS02865	98.1423	30.0066	39.9707	310.1903	206.5105	192.4257	2.0373	7.2614	0.0000	0.0029	beta-galactosidase
OG1RF_10549	OG1RF_RS02885	15.9150	0.0000	3.3309	83.2218	32.6069	37.2437	2.7733	5.1351	0.0001	0.0052	PTS fructose transporter subunit IID
OG1RF_10551	OG1RF_RS02895	100.7948	138.7803	376.3905	30.2625	83.3288	53.7964	-1.8588	7.0590	0.0009	0.0315	GTP cyclohydrolase
OG1RF_10565	OG1RF_RS02965	233.4195	82.5180	66.6178	1033.9677	364.1107	662.1098	2.4125	8.6951	0.0000	0.0018	PTS cellbiose transporter subunit IIC
OG1RF_10567	OG1RF_RS02975	132.6247	30.0066	26.6471	441.3277	144.9197	277.2585	2.1551	7.5121	0.0004	0.0184	hypothetical protein (outer surface protein)
OG1RF_10585	OG1RF_RS03065	34.4824	22.5049	9.9927	85.7437	52.5334	84.8328	1.6825	5.7758	0.0011	0.0342	hypothetical protein (M protein trans-acting positive regulator)
OG1RF_10627	OG1RF_RS03265	2503.9542	3803.3312	5176.2016	10014.3554	12850.7521	8520.5260	1.4507	12.8041	0.0006	0.0248	bifunctional acetaldehyde-CoA/alcohol dehydrogenase
OG1RF_10838	OG1RF_RS04395	387.2641	457.6000	419.6920	12.6094	19.9265	8.2764	-4.8996	7.7734	0.0000	0.0000	manganese transporter
OG1RF_10839	OG1RF_RS04400	82.2273	86.2689	93.2649	2.5219	0.0000	6.2073	-4.8069	5.5680	0.0000	0.0000	universal stress protein UspA
OG1RF_10849	OG1RF_RS04450	320.9518	150.0328	266.4711	1094.4926	561.5637	678.6626	1.6552	9.0194	0.0002	0.0120	galactokinase
OG1RF_10851	OG1RF_RS04460	400.5266	315.0689	269.8020	1205.4550	570.6212	993.1648	1.4870	9.3048	0.0006	0.0221	galactose-1-phosphate uridylyltransferase
OG1RF_10859	OG1RF_RS04500	289.1218	123.7770	176.5371	991.0959	445.6280	639.3498	1.8061	8.8178	0.0001	0.0077	excinuclease ABC subunit A (Y family DNA-directed DNA polymerase)
OG1RF_10860	OG1RF_RS04505	55.7024	26.2557	53.2942	216.8810	101.4438	167.5966	1.8143	6.7839	0.0001	0.0078	hypothetical protein

OG1RF_10861	OG1RF_RS04510	34.4824	15.0033	36.6398	98.3530	72.4598	111.7310	1.6747	6.0889	0.0004	0.0182	hypothetical protein
OG1RF_10862	OG1RF_RS04515	119.3622	75.0164	99.9267	257.2310	231.8715	285.5349	1.3836	7.5312	0.0006	0.0248	hypothetical protein
OG1RF_10870	OG1RF_RS04555	132.6247	157.5344	136.5665	360.6278	507.2189	502.7897	1.6850	8.2613	0.0000	0.0027	cell wall surface anchor protein (ebpA)
OG1RF_10871	OG1RF_RS04560	161.8021	311.3180	236.4931	491.7651	833.2881	755.2190	1.5567	8.8831	0.0003	0.0149	cell wall surface anchor protein (ebpB)
OG1RF_10874	OG1RF_RS04575	42.4399	71.2656	86.6031	7.5656	19.9265	18.6218	-2.0480	5.4664	0.0001	0.0061	DUF378 domain-containing protein
OG1RF_10910	OG1RF_RS04755	58.3549	176.2885	266.4711	17.6531	47.0989	2.0691	-2.8636	6.5904	0.0001	0.0052	CBS domain-containing protein
OG1RF_10911	OG1RF_RS04760	84.8798	183.7902	229.8313	22.6969	41.6644	24.8291	-2.4465	6.6443	0.0000	0.0002	2,3,4,5-tetrahydropyridine-2,6-dicarboxylate N-acetyltransferase
OG1RF_10912	OG1RF_RS04765	92.8373	93.7705	119.9120	17.6531	39.8529	24.8291	-1.8562	6.0907	0.0001	0.0041	acetyldiaminopimelate deacetylase
OG1RF_10993	OG1RF_RS05165	7.9575	30.0066	46.6324	2.5219	1.8115	2.0691	-3.5309	4.2002	0.0001	0.0075	spermidine/putrescine ABC transporter substrate-binding protein
OG1RF_10995	OG1RF_RS05175	23.8724	22.5049	29.9780	5.0437	3.6230	4.1382	-2.5126	4.2291	0.0002	0.0082	amidohydrolase
OG1RF_11012	OG1RF_RS05265	5.3050	3.7508	3.3309	20.1750	23.5494	24.8291	2.3575	4.2929	0.0018	0.0475	DUF5067 domain-containing protein
OG1RF_11036	OG1RF_RS05385	1562.3189	978.9639	769.4354	363.1496	461.9315	333.1240	-1.5149	9.5479	0.0004	0.0164	ATPase P (E1-E2 family cation-transporting ATPase)
OG1RF_11050	OG1RF_RS05450	87.5323	191.2918	173.2062	42.8718	67.0253	55.8655	-1.4239	6.7270	0.0018	0.0475	DNA replication protein DnaI
OG1RF_11058	OG1RF_RS05490	1501.3115	3158.1902	2081.8057	423.6746	742.7133	643.4880	-1.8948	10.4789	0.0000	0.0019	hypothetical protein
OG1RF_11059	OG1RF_RS05495	273.2069	675.1475	516.2878	95.8312	141.2967	142.7674	-1.9372	8.2731	0.0000	0.0020	tail protein
OG1RF_11060	OG1RF_RS05500	713.5208	1462.8197	959.2961	216.8810	355.0532	347.6077	-1.7653	9.4052	0.0001	0.0041	structural protein
OG1RF_11061	OG1RF_RS05505	1042.4301	2085.4557	1488.9074	421.1527	514.4648	562.7934	-1.6212	9.9964	0.0001	0.0065	hypothetical protein
OG1RF_11062	OG1RF_RS05510	363.3917	510.1115	393.0449	148.7905	126.8047	215.1857	-1.3647	8.2088	0.0009	0.0315	holin
OG1RF_11063	OG1RF_RS05515	572.9387	1211.5148	1009.2594	199.2279	251.7979	252.4294	-1.9852	9.1916	0.0000	0.0006	N-acetylmuramoyl-L-alanine amidase
OG1RF_11167	OG1RF_RS06055	106.0998	82.5180	99.9267	274.8841	201.0760	244.1530	1.3095	7.4482	0.0012	0.0362	alanine--tRNA ligase
OG1RF_11246	OG1RF_RS06450	18647.0316	2726.8459	3350.8744	2047.7604	1758.9626	2296.6935	-2.0184	12.3283	0.0014	0.0406	type I glyceraldehyde-3-phosphate dehydrogenase
OG1RF_11269	OG1RF_RS06565	1973.4554	4403.4623	7431.2136	1412.2486	1068.7826	1154.5540	-1.9250	11.5063	0.0001	0.0060	transcriptional regulator (DNA-binding protein HU)
OG1RF_11379	OG1RF_RS07115	1729.4260	1331.5410	1462.2603	615.3369	579.6787	655.9026	-1.2893	10.0579	0.0008	0.0274	oxidoreductase
OG1RF_11400	OG1RF_RS07215	156.4971	101.2721	113.2502	469.0683	210.1335	343.4695	1.4507	7.8997	0.0011	0.0343	adenine phosphoribosyltransferase
OG1RF_11437	OG1RF_RS07400	156.4971	273.8098	406.3685	98.3530	105.0668	88.9710	-1.5094	7.5769	0.0008	0.0279	cold-shock protein
OG1RF_11489	OG1RF_RS07650	2697.5862	1155.2525	1785.3566	52.9593	32.6069	35.1746	-5.5472	9.9098	0.0000	0.0000	phosphoribosylamine--glycine ligase
OG1RF_11490	OG1RF_RS07655	1917.7530	933.9541	909.3327	47.9156	23.5494	55.8655	-4.8856	9.3450	0.0000	0.0000	bifunctional phosphoribosylaminoimidazolecarboxamide formyltransferase/inosine monophosphate cyclohydrolase
OG1RF_11491	OG1RF_RS07660	400.5266	157.5344	173.2062	20.1750	1.8115	10.3455	-4.5388	7.0238	0.0000	0.0000	phosphoribosylglycinamide formyltransferase

OG1RF_11492	OG1RF_RS07665	270.5544	168.7869	179.8680	10.0875	5.4345	4.1382	-4.9605	6.7653	0.0000	0.0000	phosphoribosylformylglycinamidine cyclo-ligase
OG1RF_11493	OG1RF_RS07670	374.0016	206.2951	256.4785	25.2187	10.8690	12.4146	-4.1262	7.2284	0.0000	0.0000	amidophosphoribosyltransferase
OG1RF_11494	OG1RF_RS07675	631.2935	266.3082	266.4711	7.5656	19.9265	22.7600	-4.4845	7.6805	0.0000	0.0000	phosphoribosylformylglycinamidine synthase II
OG1RF_11495	OG1RF_RS07680	196.2845	78.7672	99.9267	12.6094	3.6230	14.4837	-3.6189	6.1465	0.0000	0.0000	phosphoribosylformylglycinamidine synthase subunit PurQ
OG1RF_11496	OG1RF_RS07685	18.5675	22.5049	19.9853	0.0000	0.0000	0.0000	-6.0205	3.7993	0.0000	0.0003	phosphoribosylformylglycinamidine synthase
OG1RF_11497	OG1RF_RS07690	76.9223	18.7541	3.3309	7.5656	0.0000	2.0691	-3.3788	4.4932	0.0015	0.0432	phosphoribosylaminoimidazolesuccinocarboxamide synthase
OG1RF_11498	OG1RF_RS07695	127.3197	37.5082	33.3089	27.7406	5.4345	6.2073	-2.3806	5.4484	0.0015	0.0424	5-(carboxyamino)imidazole ribonucleotide synthase
OG1RF_11506	OG1RF_RS07735	209.5470	311.3180	469.6554	88.2655	157.6001	111.7310	-1.4594	7.8308	0.0012	0.0358	hypothetical protein (putative lipoprotein)
OG1RF_11519	OG1RF_RS07800	34.4824	93.7705	66.6178	10.0875	18.1150	4.1382	-2.5097	5.3395	0.0000	0.0031	universal stress protein A
OG1RF_11564	OG1RF_RS08025	259.9444	367.5803	906.0018	100.8749	110.5013	82.7637	-2.3767	8.2599	0.0000	0.0005	50S ribosomal protein L19
OG1RF_11576	OG1RF_RS08085	37.1349	48.7607	109.9193	22.6969	14.4920	18.6218	-1.8012	5.4978	0.0016	0.0434	membrane protein
OG1RF_11584	OG1RF_RS08125	31.8299	56.2623	66.6178	174.0092	146.7312	167.5966	1.6689	6.8297	0.0002	0.0096	C4-dicarboxylate ABC transporter (C4-dicarboxylate anaerobic carrier)
OG1RF_11677	OG1RF_RS08600	135.2772	150.0328	139.8973	7.5656	12.6805	6.2073	-3.9282	6.2738	0.0000	0.0000	ABC transporter ATP-binding protein
OG1RF_11678	OG1RF_RS08605	108.7522	93.7705	66.6178	7.5656	28.9839	8.2764	-2.5118	5.7973	0.0000	0.0004	membrane protein
OG1RF_11679	OG1RF_RS08610	907.1529	2096.7082	2891.2117	27.7406	27.1724	16.5527	-6.3493	9.9577	0.0000	0.0000	manganese ABC transporter substrate-binding protein
OG1RF_11749	OG1RF_RS08955	973.4652	1204.0131	1825.3272	602.7275	489.1039	546.2406	-1.2886	9.8813	0.0016	0.0442	hypothetical protein
OG1RF_11752	OG1RF_RS08970	42.4399	11.2525	19.9853	131.1374	56.1564	74.4874	1.7552	5.9621	0.0011	0.0342	hypothetical protein
OG1RF_11753	OG1RF_RS08975	458.8814	603.8820	649.5234	1621.5640	1345.9415	1309.7360	1.3213	9.9727	0.0007	0.0268	PTS maltose transporter subunit IIBC
OG1RF_11774	OG1RF_RS09080	63.6599	45.0098	83.2722	292.5372	271.7244	256.5676	2.0848	7.4603	0.0000	0.0002	sugar ABC transporter substrate-binding protein
OG1RF_11775	OG1RF_RS09085	74.2698	41.2590	96.5958	378.2809	239.1175	246.2221	2.0099	7.5416	0.0000	0.0014	glucuronyl hydrolase
OG1RF_11776	OG1RF_RS09090	236.0720	367.5803	546.2658	1518.1672	1068.7826	1222.8341	1.7293	9.7030	0.0001	0.0050	hypothetical protein
OG1RF_11778	OG1RF_RS09100	400.5266	247.5541	326.4271	781.7805	661.1960	989.0266	1.3152	9.1666	0.0012	0.0367	LacI family transcriptional regulator
OG1RF_11794	OG1RF_RS09180	119.3622	26.2557	43.3016	264.7966	210.1335	184.1493	1.7648	7.2150	0.0005	0.0212	hypothetical protein
OG1RF_11860	OG1RF_RS09520	193.6320	135.0295	229.8313	22.6969	32.6069	28.9673	-2.7058	6.7797	0.0000	0.0000	guanosine monophosphate reductase
OG1RF_11976	OG1RF_RS10110	599.4636	303.8164	373.0596	2080.5448	746.3363	1390.4307	1.7199	9.8493	0.0003	0.0140	PTS beta-glucoside transporter subunit EIIBCA
OG1RF_12046	OG1RF_RS10465	448.2715	933.9541	1515.5545	146.2686	447.4395	258.6367	-1.7602	9.2931	0.0009	0.0315	adapter protein MecA
OG1RF_12070	OG1RF_RS10590	39.7874	82.5180	196.5225	25.2187	38.0414	18.6218	-1.9329	6.1199	0.0012	0.0373	hypothetical protein
OG1RF_12078	OG1RF_RS10630	18.5675	26.2557	29.9780	78.1780	65.2139	72.4183	1.5324	5.7721	0.0011	0.0342	AraC family transcriptional regulator
OG1RF_12143	OG1RF_RS10965	68.9648	157.5344	149.8900	55.4812	27.1724	37.2437	-1.6493	6.4149	0.0007	0.0265	DUF3042 domain-containing protein

OG1RF_12243	OG1RF_RS11490	124.6672	161.2852	129.9047	388.3684	260.8554	492.4442	1.4575	8.0563	0.0005	0.0217	D-ribose pyranase
OG1RF_12244	OG1RF_RS11495	302.3843	397.5869	356.4051	859.9585	722.7869	1051.0994	1.3189	9.2800	0.0009	0.0315	ribokinase
OG1RF_12280	OG1RF_RS11675	10.6100	15.0033	9.9927	100.8749	47.0989	57.9346	2.5045	5.5431	0.0000	0.0020	allantoin permease
OG1RF_12310	OG1RF_RS11830	95.4898	75.0164	99.9267	10.0875	52.5334	16.5527	-1.7225	5.9557	0.0013	0.0397	peptidase
OG1RF_12328	OG1RF_RS11925	50.3974	153.7836	303.1109	20.1750	50.7219	26.8982	-2.3421	6.6853	0.0001	0.0080	hypothetical protein
OG1RF_12393	OG1RF_RS12260	164.4546	183.7902	343.0816	73.1343	67.0253	47.5891	-1.8762	7.2214	0.0000	0.0031	hypothetical protein
OG1RF_12425	OG1RF_RS12410	503.9738	341.3246	346.4125	1684.6108	912.9939	1247.6632	1.6862	9.7253	0.0001	0.0044	glycosyl hydrolase
OG1RF_12461	OG1RF_RS12570	47.7449	45.0098	46.6324	110.9624	481.8579	157.2511	2.4236	7.2917	0.0000	0.0023	murein hydrolase regulator LrgA

Supplementary Table 2. Strains used in this study.

	Strain name	Relevant characteristics	Plasmid Source	Plasmid made	References
E. faecalis **laboratory strain**	*E. faecalis* OG1RF wild type	Laboratory strain, Rif^R, Fus^R	-	-	[1]
E. faecalis **markerless, in-frame chromosomal mutants**	OG1RF *ΔebpABC*	*ebpABC* triple deletion mutant; Rif^R, Fus^R	-	-	[2,3]
	OG1RF *ΔebpA*	*ebpA* single deletion mutant; Rif^R, Fus^R	-	-	[2,3]
	OG1RF Δ*ebpB*	*ebpB* single deletion mutant; Rif^R, Fus^R	-	-	[2,3]
	OG1RF Δ*ebpC*	*ebpC* single deletion mutant; Rif^R, Fus^R	-	-	[2,3]
	OG1RF *ndh3::*Tn *ΔmenB*	*menB* in-frame deletion with insertional mutation of *ndh3*	pGCP213	pGCP213::*delta_menB*	This study
E. faecalis **chromosomal pilin mutant**	OG1RF $ebpA^{AWAGA}$ (MIDAS)	ebpA allelic replacement with $ebpA^{AWAGA}$ (coding for Ala^{315}-Trp-Ala^{317}-Gly-Ala^{319}); Rif^R, Fus^R	-	-	[2,3]
E. faecalis **transposon mutants**	OG1RF *menB*::Tn	Rif^R, Fus^R, Cm^R (Insertional position 5' – 3': 343473)	-	-	[4,5]
	OG1RF *ndh3*::Tn	Rif^R, Fus^R, Cm^R (Insertion position 5' – 3': 2658965)	-	-	[4,5]
	OG1RF *ldh1*::Tn	Rif^R, Fus^R, Cm^R (Insertion position 5' – 3': 197152)	-	-	[4-6]
	OG1RF_RS12785-12815::Tn	Rif^R, Fus^R, Cm^R (*RS12785* Insertion position 5' – 3': 2654550) (*RS12795* Insertion position 5' – 3': 2657169) (*RS12800* Insertion position 5' – 3': 2658965) (*RS12805* Insertion position 5' – 3': 2660151) (*RS12810* Insertion position 5' – 3': 2660397) (*RS12815* Insertion position 5' – 3': 2660975)	-	-	[4,5]
	OG1RF_RS01800-01825::Tn	Rif^R, Fus^R, Cm^R (*RS01800* Insertion position 5' – 3': 343437) (*RS01805* Insertion position 5' – 3': 343749) (*RS01820* Insertion position 5' – 3': 348095) (*RS01825* Insertion position 5' – 3': 349226)	-	-	[4,5]
E. faecalis **strains with empty vector**	OG1RF *ΔebpABC*	*ebpABC* triple deletion mutant; Rif^R, Fus^R,Kan^R	pGCP123	-	[2,3]
	OG1RF wild type	Laboratory strain, Rif^R, Fus^R,Kan^R	pGCP123	-	This study

	OG1RF *menB*::Tn	Rif^R, Fus^R, Erm^R	pMSP3535	-	This study
	OG1RF *ndh3*::Tn	Rif^R, Fus^R, Erm^R	pMSP3535	-	This study
	OG1RF *ldh1*::Tn	Rif^R, Fus^R, Erm^R	pMSP3535	-	[6]
***E. faecalis* mutants with gene complementation**	OG1RF *ΔebpABC*	Complement mutation; Rif^R, Fus^R ,Kan^R	*gcp123::ebpABCsrtC*		[2,3]
	OG1RF *menB*::Tn	Complement mutation; Rif^R, Fus^R ,Erm^R	pMSP3535	pMSP3535::*menB*	This study
	OG1RF *ndh3*::Tn	Complement mutation; Rif^R, Fus^R ,Erm^R	pMSP3535	pMSP3535::*ndh3*	This study
	OG1RF *ldh1*::Tn	Complement mutation; Rif^R, Fus^R ,Erm^R	pMSP3535	pMSP3535::*ldh1*	[6]

1 Bourgogne, A. *et al.* Large scale variation in *Enterococcus faecalis* illustrated by the genome analysis of strain OG1RF. *Genome biology* **9**, R110, doi:10.1186/gb-2008-9-7-r110 (2008).

2 Nielsen, H. V. *et al.* Pilin and sortase residues critical for endocarditis- and biofilm-associated pilus biogenesis in *Enterococcus faecalis*. *Journal of bacteriology* **195**, 4484-4495, doi:10.1128/jb.00451-13 (2013).

3 Nielsen, H. V. *et al.* The metal ion-dependent adhesion site motif of the *Enterococcus faecalis* EbpA pilin mediates pilus function in catheter-associated urinary tract infection. *mBio* **3**, e00177-00112, doi:10.1128/mBio.00177-12 (2012).

4 Kristich, C. J. *et al.* Development and use of an efficient system for random mariner transposon mutagenesis to identify novel genetic determinants of biofilm formation in the core *Enterococcus faecalis* genome. *Appl Environ Microbiol* **74**, 3377-3386, doi:10.1128/aem.02665-07 (2008).

5 Dale, J. L. *et al.* Comprehensive Functional Analysis of the *Enterococcus faecalis* Core Genome Using an Ordered, Sequence-Defined Collection of Insertional Mutations in Strain OG1RF. *mSystems* **3**, doi:10.1128/mSystems.00062-18 (2018).

6 Keogh, D. *et al.* Extracellular Electron Transfer Powers *Enterococcus faecalis* Biofilm Metabolism. *mBio* **9**, doi:10.1128/mBio.00626-17 (2018).

Supplementary Table 3. Primers used in this study.

	Primer name	Primer sequence (5' → 3')	Restriction sites[a]	References
Primers used to generate complement plasmids	ndh3_F'	GGATCCAAGGAGCGGATTGTCAA	BamHI	This study
	ndh3_R'	ACTAGTGCTCGTAGTTGTCAATCGAT	SpeI	This study
	ndh3_F'_Infusion	GACTCTGCATGGATCCGGATCCAAGGAGCGGAT	BamHI	This study
	ndh3_R'_Infusion	GCAGCCCGGGACTAGTACTAGTGCTCGTAGTTGTCAA	SpeI	This study
	menB_F'	GGATCCTTTCTCTAAAGTGCCGAT	BamHI	This study
	menB_R'	ACTAGTTGTTTATTTAACCAAGTCATTGG	SpeI	This study
	menB_F'_Infusion	GACTCTGCATGGATCCGGATCCTTTCTCTAAAGTGCC	BamHI	This study
	menB_R'_Infusion	GCAGCCCGGGACTAGTACTAGTTGTTTATTTAACCAAGTCATT	SpeI	This study
Primers used to generate chromosomal deletion strain	IFD_menB_Frag1_F'	TCTCTAAAACCAATGACTTGGTTAAATAAAC	-	This study
	IFD_menB_Frag1_R'	GGCGGCCGTTACTAGTCAAATGCGTATTTAAAAATAATAACTCTTTCC	SpeI	This study
	IFD_menB_Frag2_F'	TACCGAGCTCGGATCCAAGATGCCGTTTAAGCCTC	BamHI	This study
	IFD_menB_Frag2_R'	CATTGGTTTTAGAGAAAAAGTCGCTTGAATTTTAAGA	-	This study
Primers used in qRT-PCR	gyrA_F'	TGTTCGTCGGGATGTGAGTG		[1,2]
	gyrA_R'	GGTACGCCTTTTTCGATGGC		[1,2]
	ebpR_F'	TAAACAGCGTTGGGGCGAAA		[1]
	ebpR_R'	TGGGTGGTCGTTGACGTTTT		[1]
	ebpC_F'	CGGTCATACCGACGACCAAA		[1]
	ebpC_R'	TGTCACATCGCCATCGACTT		[1]
	srtA_F'	TCGTACGCCGTTAGCAAGTT		This study
	srtA_R'	TTCATCACCGCTTCTGTGCT		This study
	srtC_F'	ACACATGCGGTCATTTCAGG		This study
	srtC_R'	GCGTCTTCCCATTGACTTCG		This study
	argR3_F'	CCACTATTTACAAGAAAAGGGCGT		This study
	argR3_R'	CGCGAGAAATCGTTGCTTGT		This study

[a] Restriction sites are underlined in the primer sequence.

1 Afonina, I., Lim, X. N., Tan, R. & Kline, K. A. Planktonic Interference and Biofilm Alliance between Aggregation Substance and Endocarditis- and Biofilm-Associated Pili in *Enterococcus faecalis*. *Journal of bacteriology* **200**, doi:10.1128/jb.00361-18 (2018).

2 Bourgogne, A. *et al.* EbpR is important for biofilm formation by activating expression of the endocarditis and biofilm-associated pilus operon (ebpABC) of *Enterococcus faecalis* OG1RF. *Journal of bacteriology* **189**, 6490-6493, doi:10.1128/jb.00594-07 (2007).